VE-PTP inhibition stabilizes endothelial junctions by activating FGD5

Laura J Braun[1], Maren Zinnhardt[1], Matthias Vockel[1,†], Hannes C Drexler[1], Kevin Peters[2] & Dietmar Vestweber[1,*] (ID)

Abstract

Inhibition of VE-PTP, an endothelial receptor-type tyrosine phosphatase, triggers phosphorylation of the tyrosine kinase receptor Tie-2, which leads to the suppression of inflammation-induced vascular permeability. Analyzing the underlying mechanism, we show here that inhibition of VE-PTP and activation of Tie-2 induce tyrosine phosphorylation of FGD5, a GTPase exchange factor (GEF) for Cdc42, and stimulate its translocation to cell contacts. Interfering with the expression of FGD5 blocks the junction-stabilizing effect of VE-PTP inhibition *in vitro* and *in vivo*. Likewise, FGD5 is required for strengthening cortical actin bundles and inhibiting radial stress fiber formation, which are each stimulated by VE-PTP inhibition. We identify Y820 of FGD5 as the direct substrate for VE-PTP. The phosphorylation of FGD5-Y820 is required for the stabilization of endothelial junctions and for the activation of Cdc42 by VE-PTP inhibition but is dispensable for the recruitment of FGD5 to endothelial cell contacts. Thus, activation of FGD5 is a two-step process that comprises membrane recruitment and phosphorylation of Y820. These steps are necessary for the junction-stabilizing effect stimulated by VE-PTP inhibition and Tie-2 activation.

Introduction

Endothelial cells determine the permeability of the blood vessel wall and thereby control extravasation of solutes, macromolecules, and leukocytes. During inflammation, vascular permeability is locally increased in the microcirculation, which enables plasma proteins and leukocytes to fight infections. However, hyperpermeability causes severe consequences in diseases such as diabetes and can be catastrophic in acute settings such as stroke, myocardial infarction, or acute respiratory distress syndrome.

Molecular mechanisms that enhance vascular permeability in inflammatory settings target specifically junctions between endothelial cells. Endothelial junction integrity relies on several adhesion molecules among which vascular endothelial (VE)-cadherin is of major importance [1–3]. It is essential for the formation of these junctions and the entire vascular system during embryonic development [4,5]. Interference with the function of VE-cadherin by adhesion-blocking antibodies is sufficient to enhance leukocyte extravasation [6] and vascular permeability [7] *in vivo*, and enhancing the interaction of VE-cadherin with the actin cytoskeleton blocked both of these processes [8]. However, when different organs were compared it was found that adhesion-blocking antibodies [7] and the conditional inactivation of the VE-cadherin gene [9] were sufficient to enhance vascular permeability in some, but not in all, organs of the mouse. Even the structural integrity of endothelial junctions as judged by electron microscopy was not affected by ablating the VE-cadherin gene in adult mice [9].

The VE-protein tyrosine phosphatase (PTP) associates with VE-cadherin and supports its function [10,11]. Inflammatory cytokines as well as leukocytes docking to endothelium dissociate VE-PTP from VE-cadherin [11,12], a process which is required *in vivo* for the induction of enhanced vascular permeability [13]. The association of VE-PTP with VEGFR-2 is also potentially relevant for the regulation of VEGF-mediated effects on endothelial junctions [14,15].

VE-PTP also associates with Tie-2, an endothelial tyrosine kinase receptor involved in angiogenesis and vascular remodeling [16,17]. Gene inactivation of VE-PTP causes embryonic lethality at midgestation due to overactivation of Tie-2 and enhanced endothelial proliferation and vessel enlargement [17–19]. Besides vascular remodeling, Tie-2 is well known to protect the vasculature against plasma leakage induced by various pro-inflammatory mediators [20–22]. The importance of VE-PTP for this junction-protective effect of Tie-2 was first suggested by the beneficial effect of the VE-PTP inhibitor AKB-9778 in mouse models of retinopathy. The inhibitor suppressed ocular neovascularization and blocked VEGF-induced vascular leakage and retinal detachment [23].

1 Max Planck Institute of Molecular Biomedicine, Münster, Germany
2 Aerpio Pharmaceuticals, Cincinnati, OH, USA
  *Corresponding author. Tel: +49 251 70365 210; Fax: +49 251 70365 299; E-mail: vestweb@mpi-muenster.mpg.de
  †Present address: Institute for Human Genetics, University of Münster, Münster, Germany

Directly comparing the effects of VE-PTP on VE-cadherin and on Tie-2 in the adult mouse, we found recently that the inhibitor AKB-9778 as well as conditional gene inactivation of VE-PTP could counteract histamine, VEGF, and LPS-induced vascular permeability in various organs. This effect was mediated by Tie-2, since it was strongly reduced upon silencing the expression of Tie-2 in these mice [9]. Of note, baseline vascular permeability was enhanced by the VE-PTP inhibitor *in vivo* in the absence of Tie-2, revealing the supportive effect of VE-PTP on VE-cadherin under these conditions. Thus, inhibition of VE-PTP *in vivo* has opposing effects on endothelial junctions due to its different effects on VE-cadherin and on Tie-2. However, activation of Tie-2 via inhibition of VE-PTP protects endothelial junctions against inflammation-induced destabilization and even overrides the negative effect of VE-PTP inhibition on the junction-stabilizing function of VE-cadherin [9].

Mechanistically, Tie-2 signaling was suggested to counteract VEGF-induced permeability across endothelial monolayers by blocking VE-cadherin endocytosis [24]. In addition, it was shown that the Tie-2 ligand angiopoietin-1 (Ang1) activated the GTPase Rac1 which in turn blocked the activation of RhoA and thereby relieved the pulling forces of actomyosin radial stress fibers (RSF) on endothelial junctions [22,25]. We could confirm this and found that the activation of Rap1 is an additional essential signaling step downstream of Tie-2 and upstream of Rac1 activation in this pathway [9]. Rap1 is a well-characterized GTPase known to enhance the stability of endothelial junctions [26–29]. Stimulation of the GEF Epac1 by pharmacologically enhancing intracellular cAMP levels or by a cAMP analogue (007) triggers the activation of Rap1, enhances the formation and tension of junction-stabilizing circumferential actin bundles (CAB), and reduces pulling forces on junctions by counteracting RSF formation [30–33].

FGD (FYVE, RhoGEF, and PH domain containing) 5 is a GEF of Cdc42 and belongs to the FGD GEF family that contains FGD1 to FGD6 as well as the FGD1-related Cdc42-GEF (FRG). They all share a Dbl homology, a FYVE, and two pleckstrin homology (PH) domains. FGD5 is by far the largest member in this family containing 30 tyrosine residues in the mouse and a large N-terminus comprising about half of the molecule which is potentially unstructured. This GEF was reported to be specifically expressed in hematopoietic stem cells [34] and in endothelial cells based on *in situ* hybridization and was found to be involved in vascular pruning, endothelial cell network formation, and directional movement in the mouse embryo [35,36]. In cultured endothelial cells, it has been implicated in the stabilization of endothelial junctions, where it was acting downstream of the cAMP-Epac1-Rap1 pathway, stimulating Cdc42-dependent activation of the kinase MRCK which phosphorylated S19 of the regulatory light chain of non-muscle myosin II, stimulating junctional CAB [30]. This was reproduced by Pannekoek *et al* [33], although in this study silencing of FGD5 had only a limited effect on cAMP-Epac1-Rap1-mediated junction stabilization.

Here, we have analyzed the mechanism whereby the inhibition of VE-PTP stabilizes endothelial junctions. Searching for targets of VE-PTP, we identified FGD5 as a direct substrate. Determining which tyrosine residue is targeted by VE-PTP enabled us to show that tyrosine phosphorylation of FGD5 is required for the full activation of FGD5. We found that VE-PTP inhibition triggers enhanced FGD5 phosphorylation by blocking its dephosphorylation as well as

by activating the kinase activity of Tie-2. FGD5 was required for the junction-stabilizing effect of a VE-PTP inhibitor *in vitro* and *in vivo*. These effects were due to enhancing circumferential actin bundles as well as blocking the tension of radial stress fibers on junctions.

Results

FGD5 is a substrate of VE-PTP

In order to understand more about the mechanism of how VE-PTP modulates endothelial junction integrity, we searched for novel substrates of this tyrosine phosphatase. To this end, changes of protein phosphorylation were analyzed by comparing untreated mouse bEnd.5 cells with cells treated for 30 min with the VE-PTP inhibitor AKB-9778. Tryptic digests of cell lysates were subjected to affinity isolation on TiO_2 microspheres, and isolated phosphopeptides from each cell population were analyzed and compared by mass spectrometry. In total, 6,569 class I phosphosites could be identified across both samples measured by two methods (HCD and MSA, see Materials and Methods). Of these, 341 phosphosites were specifically detected in the AKB-9778-treated samples with a localization probability > 0.75 in both the HCD- and the MSA-based measurements, among them a considerable fraction of phosphotyrosine sites ($n = 56$, 16.4%; Dataset EV1). Several of the identified phosphosites were found in proteins that are potentially relevant for the regulation of junctions, such as FGD5, Tie-2, Tie-1, ZO-1, claudin-5, p120, VEGFR-3, JAM-C, neuropilin-1, afadin, PAR-3, ArhGAP12, and SHP-2. Since another proteomics approach showed that the Cdc42 GEF FGD5 was one of the major proteins isolated with an anti-phospho-tyrosine antibody from bEnd.5 cells after AKB-9778 treatment (Drexler *et al*, unpublished), we decided to analyze this protein further.

To verify the substrate character of FGD5, bEnd.5 mouse endothelioma cells were briefly pre-treated with peroxyvanadate, and cell lysates were subjected to pull-down assays with a GST-VE-PTP fusion protein containing the cytoplasmic tail of VE-PTP (fused to glutathione S-transferase) and an analogous protein carrying an inactivating CS/DA point mutation in the active center of the phosphatase domain. The mutation leaves substrate recognition intact, yet the phosphatase activity is lost, which strongly stabilizes the enzyme–substrate interaction. For the detection of mouse FGD5, polyclonal antibodies were raised against and purified on a recombinant form of the first 248 amino acids of FGD5 (Fig EV1). As shown in Fig 1A, the phosphatase-dead trapping mutant of VE-PTP bound strongly to FGD5, whereas binding to the WT protein was hardly stronger than to the GST-negative control. In agreement with this result, FGD5 could only be efficiently immunoprecipitated from HUVEC lysates with an anti-phospho-tyrosine antibody when these cells were pre-treated for 30 min with the VE-PTP inhibitor AKB-9785 (Fig 1B). Corresponding to this finding, knocking down VE-PTP in HUVEC by siRNA enhanced tyrosine phosphorylation of FGD5 as shown in immunoblots (Fig 1C). Subcutaneous administration of AKB-9785 in mice for 1 h followed by immunoprecipitation of FGD5 from lung lysates and subsequent anti-phospho-tyrosine immunoblotting also revealed a 3- to 3.5-fold increase in pY levels of FGD5 *in vivo* (Fig 1D). We conclude that FGD5 is a substrate of VE-PTP.
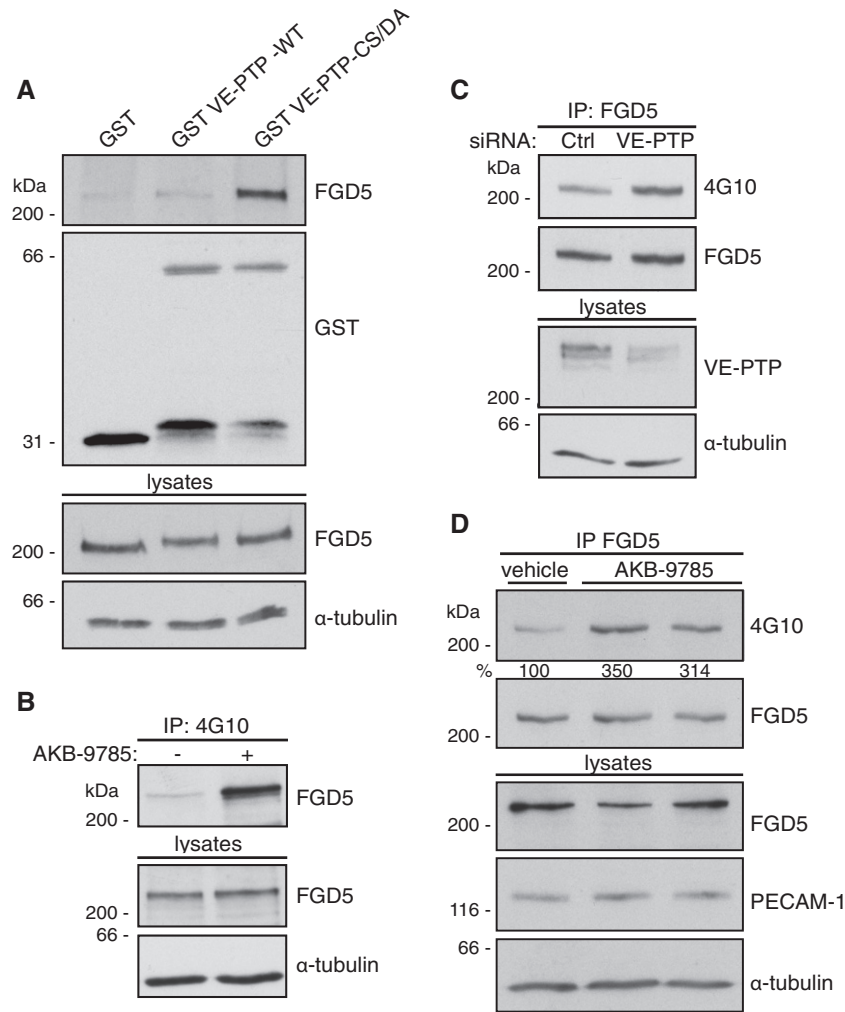
Figure 1. FGD5 is a substrate of VE-PTP.

A bEnd.5 cells were stimulated with peroxyvanadate for 7 min, lysed, pre-cleared by incubation with GST, and submitted to pulldowns with GST, GST-VE-PTP-WT, or GST-VE-PTP-CS/DA (as indicated). Pulldowns and total cell lysates were analyzed by immunoblot for FGD5, GST, and α-tubulin.

B Lysates of HUVEC treated with vehicle (−) or 5 μM AKB-9785 (+) for 30 min were submitted to immunoprecipitation (IP) with 4G10. Precipitates were immunoblotted for FGD5 and cell lysates for FGD5 and α-tubulin.

C Lysates of HUVEC transfected with VE-PTP-targeting or control siRNA were submitted to immunoprecipitation of FGD5. Precipitates and lysates were immunoblotted for phospho-tyrosines (4G10), FGD5, VE-PTP and α-tubulin.

D FGD5 was precipitated from total lung lysates of C57BL/6 mice that received subcutaneous injections of vehicle or AKB-9785 for 1 h. Precipitates and lysates were immunoblotted for phospho-tyrosines (4G10), FGD5, PECAM-1 and α-tubulin.

Data information: Results are representative of two (D) or three (A–C) independent experiments.

FGD5 translocates to cell contacts upon VE-PTP inhibition

Activation of GEFs is usually accompanied by recruitment to membranes at their site of action. For FGD5, it had been reported that it is translocated to endothelial cell contacts upon activation of the Rap1 GEF Epac1 with the cAMP analogue 8-pCPT-2′-O-Me-cAMP (007) [30]. Therefore, we tested whether inhibition of VE-PTP would have a similar effect. As shown in Fig 2A and B, AKB-9785 indeed enhanced the recruitment of FGD5 to junctions of HUVEC monolayers in a similar way as the reagent 007. At the same time, we observed a straightening of endothelial junctions (judged by staining for VE-cadherin) and reduced radial stress fibers. VE-cadherin staining levels were unchanged at cell contacts (Fig 2C). Due to the similarities of the effects, we tested whether 007 would also stimulate the phosphorylation of FGD5. However, immunoblot analysis revealed that only AKB-9785 but not 007 treatment of HUVEC triggered tyrosine phosphorylation of FGD5 (Fig 2D). This strongly suggests that tyrosine phosphorylation of FGD5 is not required for its recruitment to junctions.

We have shown recently that Tie-2 activation, induced by VE-PTP inhibition, leads to the activation of Rap1. Furthermore, Rap1 was needed for the junction-stabilizing effect of the VE-PTP inhibitor [9]. Therefore, we tested whether Rap1, although not sufficient to trigger tyrosine phosphorylation of FGD5, would be involved in

this process. To this end, we inhibited the expression of Rap1a/b in HUVEC by siRNA and re-analyzed the effects of AKB-9785 on junction recruitment and tyrosine phosphorylation of FGD5. As shown

in Fig 2G, Rap1a/b expression was largely repressed. The consequence was a strong inhibition of AKB-9785-induced junction recruitment of FGD5 (Fig 2E and F), whereas the induction of
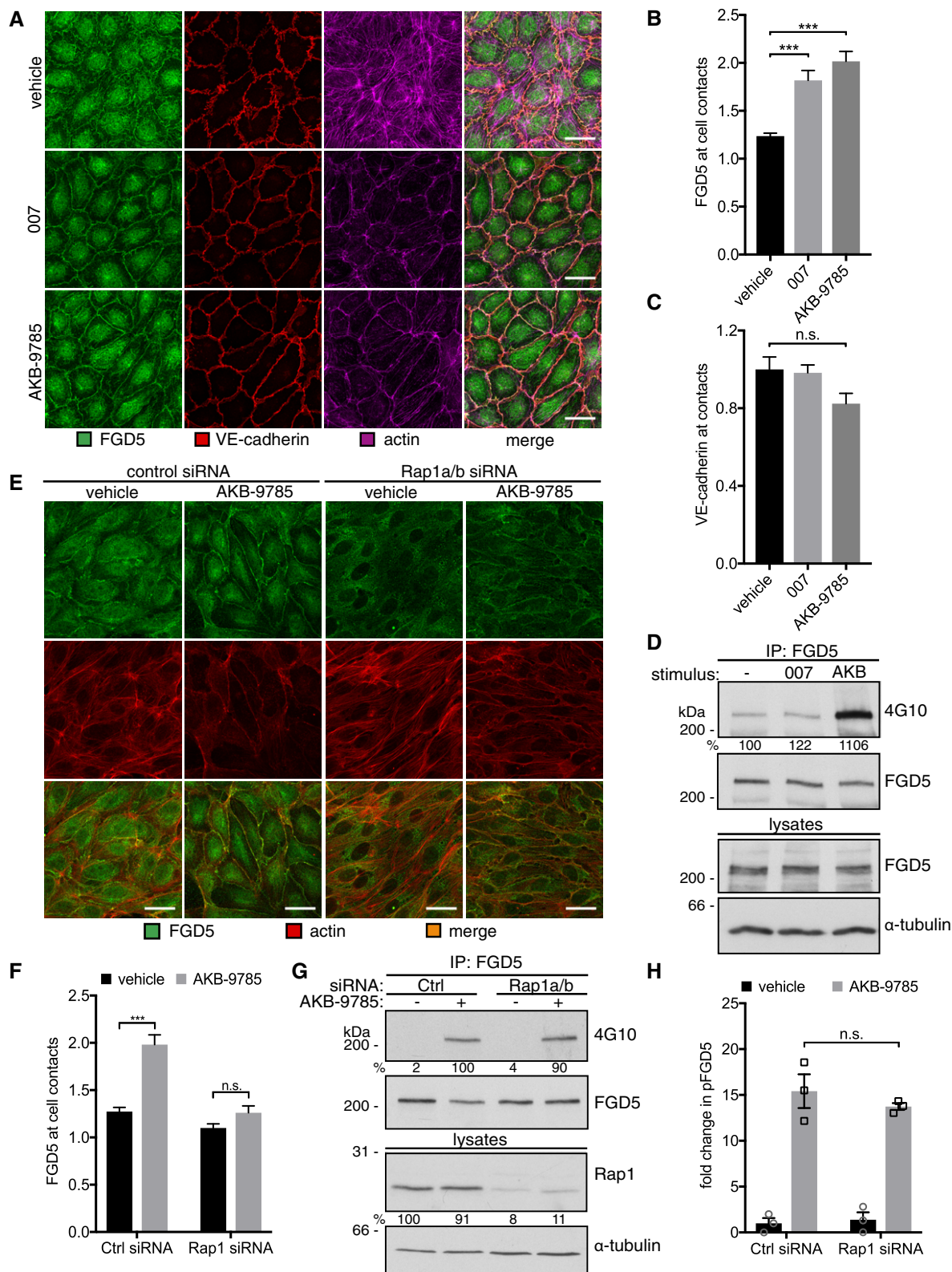

Figure 2.

Figure 2. Rap1 mediates translocation to cell contacts but not phosphorylation of FGD5 upon VE-PTP inhibition.

A Confluent HUVEC monolayers were stimulated with vehicle, 200 μM 007, or 5 μM AKB-9785 for 20 min. Cells were fixed, permeabilized, and stained for FGD5, VE-cadherin, and F-actin. Scale bars 30 μm.

B Quantification of FGD5 signal intensities at cell contacts relative to FGD5 signal intensities in adjacent areas of the cytoplasm of 20–25 cells as shown in (A).

C Quantification of VE-cadherin signals at cell–cell junctions relative to cytoplasmic signals of 20–25 cells as displayed in (A).

D FGD5 was immunoprecipitated from HUVEC lysates after stimulation with 200 μM 007 for 20 min or 5 μM AKB-9785 for 30 min. Precipitates and lysates were immunoblotted for phospho-tyrosines (4G10), FGD5, and α-tubulin.

E HUVEC were transfected with Rap1a/b-targeting or control siRNA and treated with 5 μM AKB-9785 or vehicle. Fixed and permeabilized monolayers were stained for FGD5 and F-actin. Scale bars 30 μm.

F FGD5 signal intensities at cell contacts relative to FGD5 signal intensities in the cytoplasm of 20–25 cells as shown in (E).

G FGD5 immunoprecipitates from HUVEC transfected with Rap1a/b-targeting or control siRNA and treated with 5 μM AKB-9785 or vehicle for 30 min were immunoblotted for 4G10 and FGD5, and cell lysates for Rap1 and α-tubulin.

H Quantification of 4G10 signals as shown in (G). 4G10 signal intensities are displayed relative to the amount of precipitated FGD5 in the respective sample and normalized to control siRNA- and vehicle-treated cells.

Data information: Graphs represent mean ± SEM. Results are representative of three (A, D, G) or four (E) independent experiments or pooled from three (B, C, H) or four (F) independent experiments. Statistical significance was tested using one-way (B) or two-way ANOVA (F, H) ***$P < 0.001$, n.s., not significant.

tyrosine phosphorylation was unaffected (Fig 2G and H). We conclude that Rap1 is needed for the recruitment of FGD5 to junctions upon VE-PTP inhibition, but is not involved in the tyrosine phosphorylation of FGD5 downstream of VE-PTP.

Stimulation of Tie-2 activates FGD5

Since VE-PTP inhibition stabilizes endothelial junctions by activating Tie-2 [9], we tested whether Tie-2 would be relevant for the induction of tyrosine phosphorylation of FGD5. To this end, we transfected HUVEC with siRNA targeting Tie-2 and stimulated with AKB-9785 48 h later. Western blots of immunoprecipitated FGD5 revealed a 44% reduction of phospho-tyrosine levels upon Tie-2 siRNA treatment (Fig 3A and B). Thus, either Tie-2 itself or a kinase downstream of Tie-2 is responsible for the phosphorylation of FGD5. Since inhibition of Tie-2 expression was highly efficient, it is unlikely that the remaining phosphorylation of FGD5 was due to residual Tie-2. Therefore, it cannot be excluded that another kinase is also involved in the phosphorylation of FGD5.

Next, we tested whether direct stimulation of Tie-2 with the agonist Ang1, without inhibiting VE-PTP, would also stimulate FGD5. We found that the treatment of confluent HUVEC monolayers with recombinant COMP-Ang1 was sufficient to stimulate FGD5 tyrosine phosphorylation and translocation of FGD5 to cellular junctions (Fig 3C–E). Likewise, Ang1 was able to stimulate Cdc42 activation, as was analyzed by a colorimetric Cdc42 G-LISA assay (Fig 3F). Thus, FGD5 acts downstream of Tie-2 and could be involved in the junction-stabilizing effect of this receptor.

FGD5 is required *in vitro* for the endothelial junction-stabilizing effect of VE-PTP inhibition

To analyze the functional relevance of FGD5, we tested whether inhibition of FGD5 expression would interfere with the junction-stabilizing effect induced by VE-PTP inhibition or Tie-2 activation. To this end, we transfected HUVEC with FGD5 siRNA, seeded them on Transwell filters, and tested the effect of AKB-9785 on paracellular permeability induced by thrombin. Under control siRNA conditions, thrombin-induced permeability for FITC-dextran was prevented by AKB-9785 (Fig 4A). In contrast, upon depletion of FGD5, AKB-9785 could no longer significantly compensate the permeability-enhancing effect of thrombin (Fig 4A). FGD5

expression was inhibited by siRNA by 83% as determined by immunoblot analysis (Fig 4B). Since endothelial cells also express FGD1 and FGD6, we analyzed whether FGD5 siRNA or control siRNA would interfere with the mRNA levels of FGD1, FGD5, and FGD6. We found reduction of the mRNA level solely for FGD5 (Fig 4C).

To analyze endothelial junction integrity by an alternative method, we applied the electric cell impedance sensing (ECIS) technique. Control or FGD5 siRNA-treated HUVEC were cultured on ECIS slides; treated for 30 min with COMP-Ang1, AKB-9785, or vehicle; and then exposed to thrombin. As shown in Fig 4D (direct resistance measurements in Fig EV2), COMP-Ang1 and AKB-9785 partially compensated the loss of electrical resistance caused by thrombin, whereas this compensating effect was lost when FGD5 expression was inhibited by siRNA. Thus, FGD5 is essential for the junction-stabilizing effect caused by VE-PTP inhibition or Tie-2 activation. Interestingly, FGD5 siRNA had no effect on basal permeability for FITC-dextran in Transwell filter assays (Fig 4E).

VE-PTP inhibition requires FGD5 to counteract histamine-induced vascular permeability *in vivo*

We have shown previously that VE-PTP inhibition protects *in vivo* against histamine-induced vascular permeability in the skin and that this effect was mediated by the activation of Tie-2 [9]. To analyze whether FGD5 is required for this protection against the induction of vascular permeability, we used an *in vivo* siRNA approach for FGD5. Stabilized siRNA targeting FGD5 and control siRNA were intravenously injected in combination with a polyethyleneimine-based transfection reagent, and knockdown efficiency was determined 48 h later by immunoblot analysis of lung lysates. Administration of *in vivo* FGD5 siRNA efficiently inhibited FGD5 expression by 80% (±5%) as determined for 16 mice (Fig 5A and B). The expression of endothelial markers such as VE-cadherin, Tie-2, VE-PTP, and PECAM-1 was not compromised. This siRNA approach was combined with a Miles assay for the skin. Based on i.v. injected Evans blue and intradermal challenge with histamine, we found that permeability induction was clearly reduced by AKB-9785 in mice treated with control siRNA, whereas this protective effect of AKB-9785 was largely lost in mice with blocked expression of FGD5 (Fig 5C). Silencing efficiency is documented for some of these mice in Fig 5D. These results suggest that FGD5 is required for the vascular barrier-protective effect of VE-PTP *in vivo*.
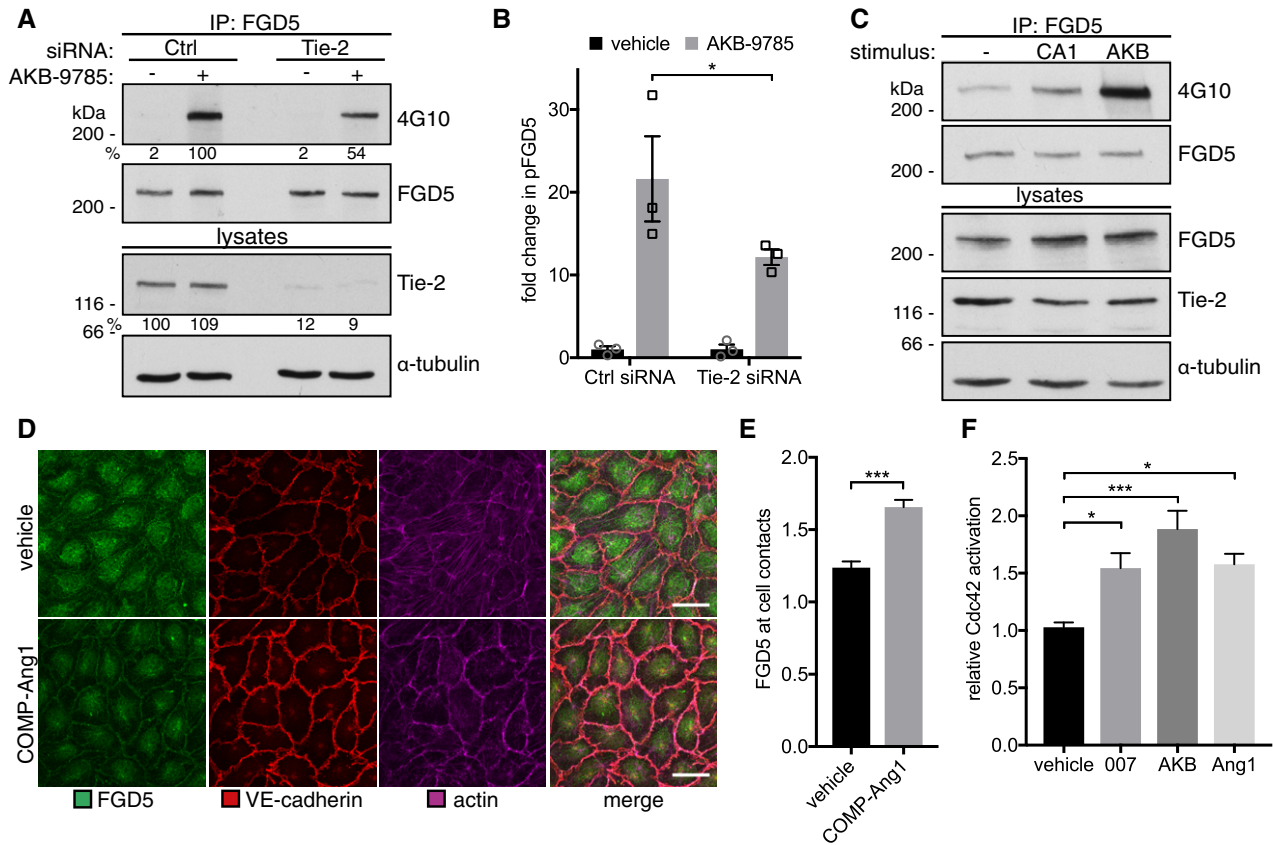
Figure 3. Tie-2 activation induces FGD5 phosphorylation, translocation, and activation of Cdc42.

A FGD5 was immunoprecipitated from HUVEC stimulated with vehicle or 5 μM AKB-9785 for 30 min after transfection with Tie-2-targeting or control siRNA. Precipitates were probed for phospho-tyrosines (4G10) and FGD5, and lysates for Tie-2 and α-tubulin.

B 4G10 signal intensities from three similar experiments as the one displayed in (A) were normalized to the amount of precipitated FGD5.

C HUVEC were starved in serum-free medium, treated with 1 μg/ml COMP-Ang1 (CA1) or 5 μM AKB-9785, followed by FGD5 immunoprecipitation and immunoblotting for phospho-tyrosines (4G10), FGD5, Tie-2, and α-tubulin.

D Confluent HUVEC monolayers were treated with 1 μg/ml COMP-Ang1 or vehicle for 20 min, and fixed, permeabilized cells were stained for FGD5, VE-cadherin, and F-actin. Scale bars 30 μm.

E Quantification of FGD5 signal intensities at cell contacts relative to FGD5 signal intensities in the cytoplasm of the same cell upon vehicle or Ang1 stimulation as in (D) with 20 cells analyzed.

F Serum-starved HUVEC were treated with 200 μM 007, 5 μM AKB-9785, 600 ng/ml Ang1, or vehicle for 20 min, and Cdc42 activation levels were compared using a colorimetric Cdc42 G-LISA activity assay.

Data information: Results are representative of three independent experiments (A, C, D) or pooled from three (B, E) or five independent experiments (F). Statistical significance was tested using one-way ANOVA. *$P < 0.05$, ***$P < 0.001$. Results are displayed as mean ± SEM.

FGD5 is required for the induction of cortical actin bundles and for the suppression of radial stress fibers

Thrombin is known to interfere with endothelial junction integrity by stimulating the formation of radial stress fibers, which exert pulling forces on junctions, and by reducing cortical actin bundles which are thought to support stabilizing effects on junctions [26,28,30]. We found that these effects are counteracted by AKB-9785. This prompted us to test whether FGD5 would be involved in these effects. To this end, HUVEC were transfected either with control siRNA or with siRNA targeting FGD5, and after pre-incubation with vehicle or with AKB-9785, cells were treated with thrombin. After fixation and permeabilization, cells were stained for actin and VE-cadherin. As shown in Fig 6A, AKB-9785 prevented the effect of thrombin on radial stress fiber formation and the

suppression of cortical actin bundles. This effect of AKB-9785 was lost if FGD5 expression was inhibited. Expression of FGD5 was reduced by 81% (Fig 6B).

It was reported that 007-induced activation of Rap1 stabilizes endothelial junctions by stimulating FGD5-dependent activation of Cdc42 which leads to the activation of the kinase MRCK which supports serine 19 (S19) phosphorylation of the regulatory light chain of non-muscle myosin II (NMII), which supports cortical actin bundle formation. In agreement with these findings, we found that AKB-9785 enhanced junctional localization of MLC-S19 (Fig EV3).

In contrast, the inhibitory effect of 007 on the formation of radial stress fibers has been explained so far by the activation of Rap1, which counteracts the activation of RhoA through ArhGAP29 [37]. A role for FGD5 has not been reported for this effect. Thus, we show here for the first time that FGD5 is needed for the inhibitory effect of
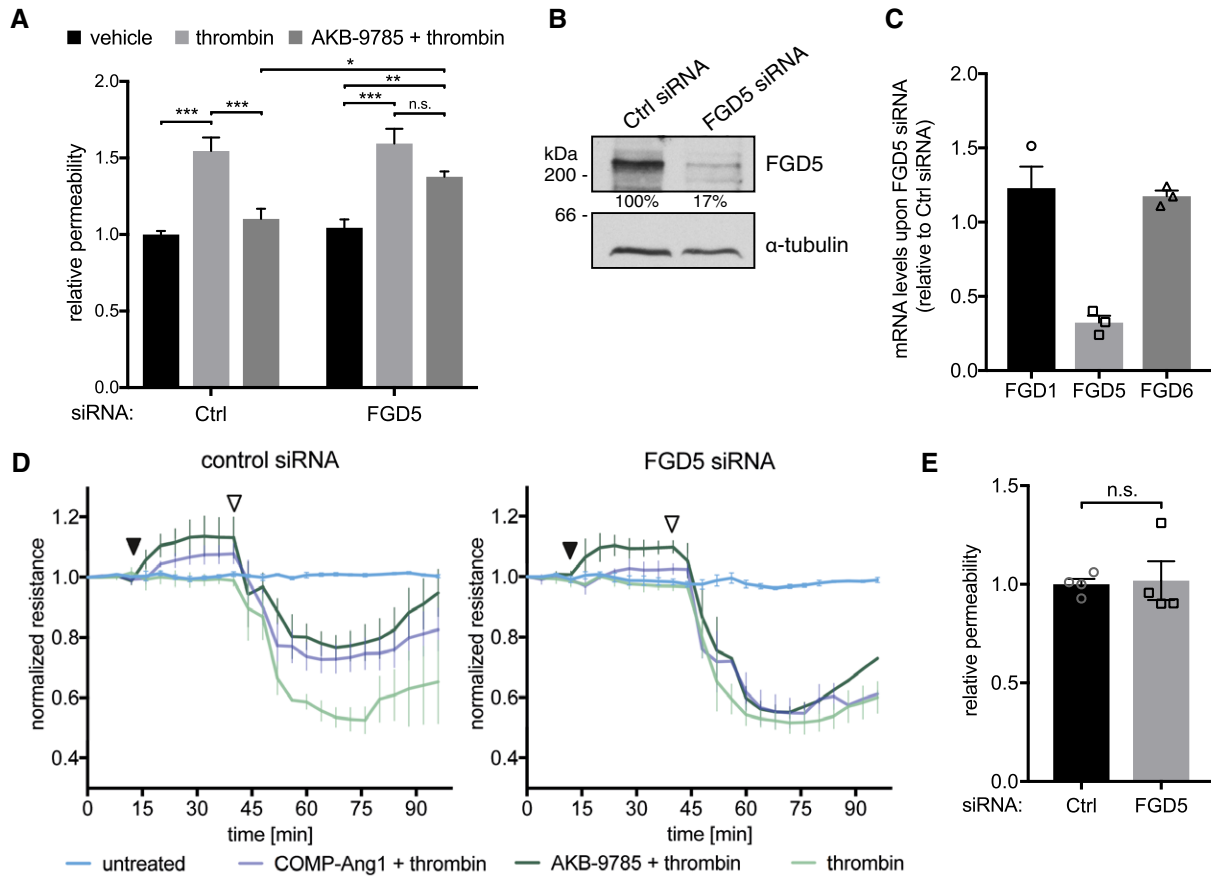
Figure 4. FGD5 is necessary to counteract thrombin-induced vascular leak induction by inhibition of VE-PTP.

A   Paracellular permeability for 250 kD FITC-dextran was determined for HUVEC transfected with FGD5-targeting or control siRNA. Cells were treated with vehicle, thrombin, or a combination of thrombin and 5 μM AKB-9785 (as indicated).

B   Total cell lysates of HUVEC transfected with control or FGD5-targeting siRNA were immunoblotted for expression of FGD5 and α-tubulin.

C   mRNA levels of FGD1, FGD5, and FGD6 in HUVEC transfected with FGD5 siRNA, represented as expression relative to control siRNA-treated cells.

D   Impedance measurements of control or FGD5 siRNA-treated HUVEC at 4,000 Hz using the ECIS ZΘ system. After pre-treatment with vehicle, 5 μM AKB-9785, or 1 μg/ml COMP-Ang1 (black arrowheads), cells were stimulated with thrombin (open arrowheads). Resistance values were normalized to the average resistance over 30 min prior to pre-treatment.

E   Paracellular permeability for 250 kD FITC-dextran of control or FGD5 siRNA-treated HUVEC under basal conditions.

Data information: Results are pooled from three (C), four (D, E), or five independent experiments with three filters per assay (A) or representative of five independent experiments (B). Statistical significance was tested using two-way ANOVA (A) or Student's *t*-test (E). *$P < 0.05$, **$P < 0.01$, ***$P < 0.001$, n.s., not significant. Results are shown as mean ± SEM.

AKB-9785 on radial stress fiber formation. In agreement with this, we found that the simultaneous phosphorylation of threonine 18 and serine 19 of MLC of NMII, which is preferentially found in radial stress fibers [30], is inhibited by AKB-9785 (Fig 6A). This effect was again lost if FGD5 expression was inhibited by siRNA (Fig 6A). Thus, AKB-9785-driven inhibition of VE-PTP stabilizes endothelial junctions by activating FGD5, which supports on the one hand the formation of circumferential actin by stimulating Cdc42 and the kinase MRCK and on the other hand by inhibiting the RhoA/ROCK-driven simultaneous phosphorylation of T18/S19 of NMII MLC and the formation of radial stress fibers.

Tie-2 was reported to inhibit radial stress fibers by activating Rac1 [22,25], and we showed previously that Tie-2 mediates these effects by activating Rap1, which then activates Rac1 [9]. Since we found here that FGD5 counteracts the formation of radial stress

fibers, we tested whether FGD5 would be needed for Tie-2-stimulated Rac1 activation. We found that silencing FGD5 in HUVEC blocked the activation of Rac1 by AKB-9785, as tested by a colorimetric Rac1 G-LISA activity assay (Fig 6C and D). Interestingly, silencing Cdc42 did not interfere with AKB-9785-stimulated activation of Rac1 (Fig 6E and F), suggesting that FGD5 acts upstream of Rac1 activation, but does not need Cdc42 for this effect.

Y820 of human FGD5 is the direct substrate of VE-PTP

Our phospho-peptide proteome analysis had revealed that out of the 30 tyrosine residues of mouse FGD5, Y576 was the only one we specifically detected in the AKB-9778-stimulated endothelial cell sample (Fig EV4). The equivalent tyrosine in the slightly larger human FGD5 (containing 34 tyrosine residues) is found at position
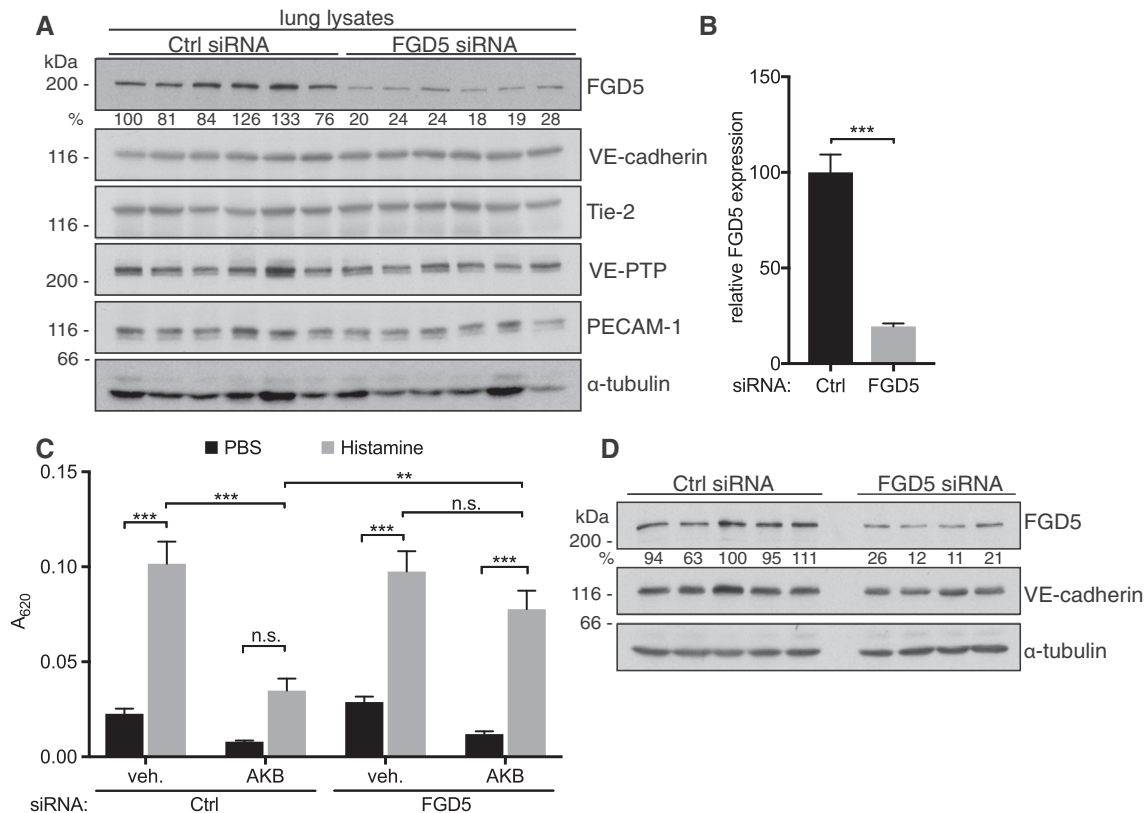
Figure 5. VE-PTP inhibition requires FGD5 to counteract histamine-induced vascular permeability in the skin.

A Total lung lysates of C57BL/6 mice i.v. injected with control or FGD5-targeting siRNA for 48 h were immunoblotted for the indicated antigens. Percentages indicate the FGD5 protein levels relative to VE-cadherin levels, with the ratio of the FGD5 and VE-cadherin signal of the first lane arbitrarily set as 100.

B The average FGD5 knockdown efficiency in murine lungs was determined by quantification of immunoblot signals for FGD5 relative to VE-cadherin of 16 control or FGD5-targeting siRNA-treated animals each.

C Mice were treated with FGD5 or control siRNA as in (A). After 48 h, they were injected subcutaneously with 0.6 mg AKB-9785 or vehicle followed by intravenous injection of Evans Blue dye 30 min later and intradermal injections of PBS or histamine another 15 min later. After 30 min, mice were sacrificed, and the dye was extracted from skin samples and quantified by measuring absorbance at 620 nm.

D Total lung lysates of mice in (C) were immunoblotted for the indicated antigens.

Data information: Data are representative of three independent experiments (A, D) or pooled from three independent experiments with 5–6 mice (B) or 3 mice per group (C). Results are displayed as mean ± SEM. Statistical significance was tested using Student's t-test (B) or two-way ANOVA (C). **$P < 0.01$, ***$P < 0.001$, n.s., not significant.

820. In order to analyze the physiological relevance of this tyrosine as a target for VE-PTP, we generated a Y820F point-mutated version of human FGD5. As additional modifications, an EGFP tag was fused to the N-terminus and three silent mutations were introduced, to allow for siRNA-insensitive expression.

To verify whether Y820 is indeed a substrate of VE-PTP, we expressed FGD5-WT-EGFP and FGD5-Y820F-EGFP in HUVEC, treated the cells without and with AKB-9785, and analyzed anti-EGFP immunoprecipitates in immunoblots for phospho-tyrosine epitopes. As shown in Fig 7A, both basal phosphorylation and AKB-9785-induced phosphorylation were largely undetectable for the Y820F mutant when compared to the WT protein. This indicates that Y820 is not only the residue, which is predominantly phosphorylated upon VE-PTP inhibition, but that it is phosphorylated under basal conditions as well.

To analyze whether pY820 is the direct substrate of VE-PTP, we performed substrate-trapping experiments, using GST-VE-PTP fusion proteins in pull-down assays, which carried the inactivating mutation CS/DA in the active center of the phosphatase domain. To test a potential VE-PTP interaction with pY820, we first blocked the expression of endogenous FGD5 by siRNA transfection of HUVEC. Seventy-two hours later, cells were transduced with adenovirus vectors expressing either FGD5-WT-EGFP or FGD5-Y820F-EGFP, followed 48 h later by a 7-min treatment with peroxyvanadate to achieve maximal phosphorylation levels of FGD5. Subsequently, we performed pull-down experiments with GST-VE-PTP, GST-VE-PTP-CS/DA, or GST as control. As shown in Fig 7B, WT-FGD5 was pulled down by the VE-PTP-trapping mutant 9 times more efficient than by the WT form of VE-PTP confirming the specific enzyme–substrate interaction between VE-PTP and FGD5 reported above (Fig 1). In contrast, Y820F-FGD5 was pulled down only 1.2 times more efficiently by the VE-PTP-trapping construct than by the WT form of VE-PTP. Thus, the interaction between FGD5 and VE-PTP, which is based on the binding of the
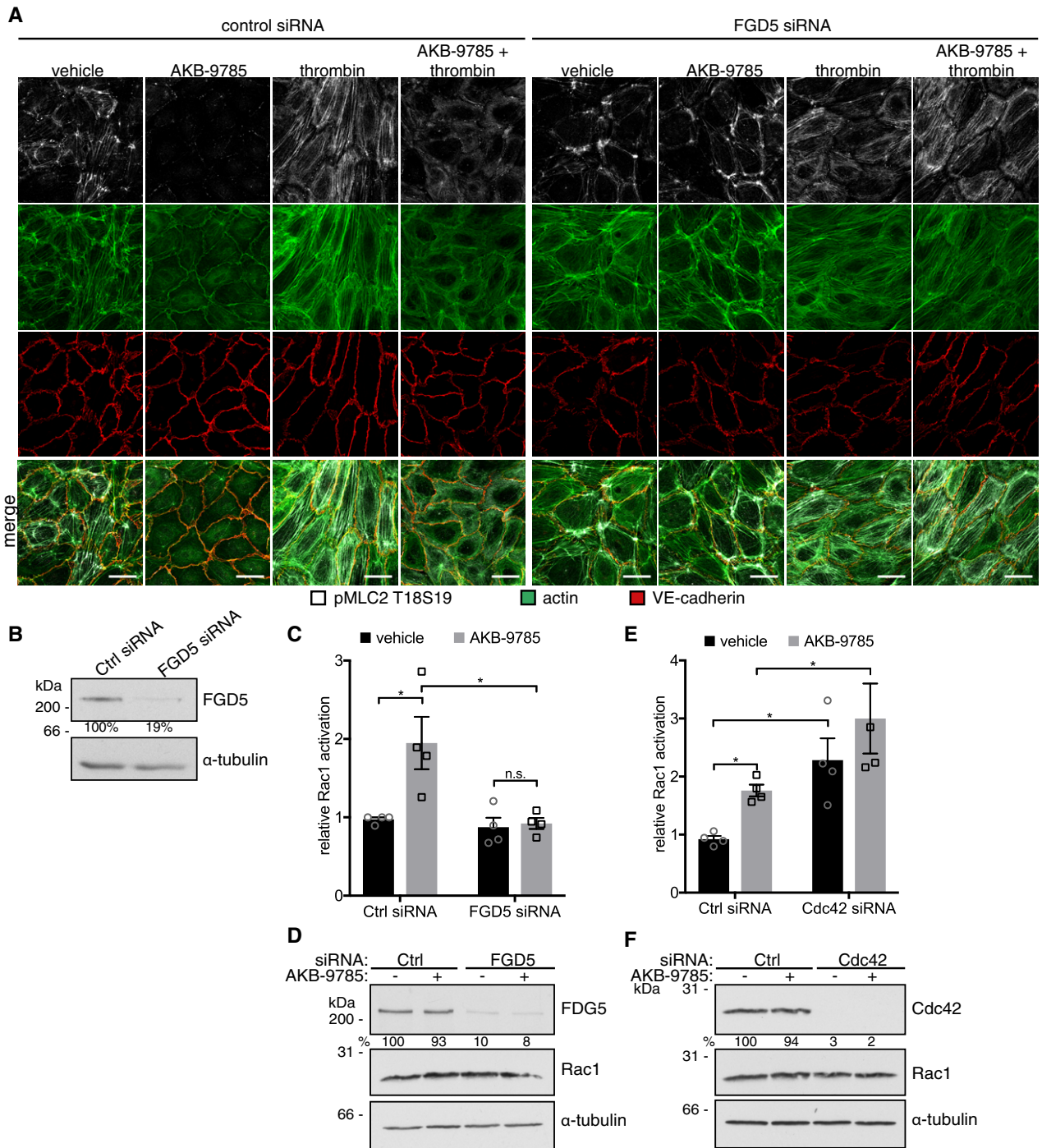
Figure 6. VE-PTP inhibition blocks thrombin-induced formation of stress fibers and strengthens the cortical actin network via FGD5.

A   Control or FGD5 siRNA-transfected confluent HUVEC monolayers were pre-treated with either vehicle or 5 μM AKB-9785 for 30 min and stimulated with thrombin for 2 min (as indicated), followed by staining of fixed, permeabilized cells for pMLC2-T18S19, VE-cadherin and F-actin. Scale bars 30 μm.

B   Total cell lysates of HUVEC transfected with control or FGD5-targeting siRNA were immunoblotted for expression of FGD5 and α-tubulin.

C   HUVEC were transfected with control or FGD5-targeting siRNA and serum-starved 72 h later, before they were treated with vehicle or 5 μM AKB-9785 for 20 min. Rac1 activation levels were compared using a colorimetric Rac1 G-LISA activity assay.

D   Lysates as used in (C) were immunoblotted for FGD5, Rac1, and α-tubulin.

E   HUVEC transfected with control or Cdc42-targeting siRNA were serum-starved and stimulated with vehicle or 5 μM AKB-9785 for 20 min. Lysates were submitted to a colorimetric Rac1 G-LISA activation assay to compare Rac1 activation levels.

F   Cell lysates as used in (E) were subjected to immunoblot analysis for Cdc42, Rac1, and α-tubulin expression.

Data information: Data are representative of (A, B, D, F) or pooled from (C, E) four independent experiments. Results are displayed as mean ± SEM. Statistical significance was tested using two-way ANOVA *$P < 0.05$.
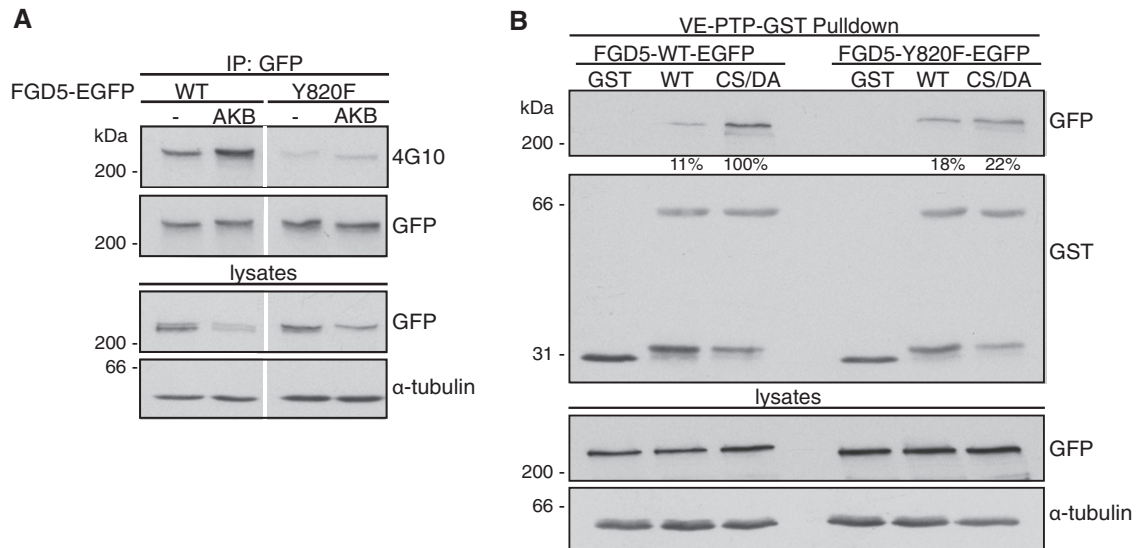
Figure 7. Y820 of FGD5 is a substrate of VE-PTP.

A HUVEC transfected with FGD5 siRNA and transduced to re-express FGD5-WT-EGFP or FGD5-Y820F-EGFP were treated with 5 μM AKB-9785 or vehicle for 30 min. GFP precipitates and lysates were immunoblotted for phospho-tyrosines (4G10), GFP, and α-tubulin.

B Lysates of HUVEC, siRNA treated and transduced as in (A) and treated with peroxyvanadate for 7 min, were pre-cleared by incubation with GST and submitted to pulldowns with GST, GST-VE-PTP-WT, or GST-VE-PTP-CS/DA (as indicated). Pulldowns and total cell lysates were immunoblotted for GFP, GST, and α-tubulin. Percentages indicate the signal intensities of GFP in the respective lane relative to the signal intensity of FGD5-WT pulled down by VE-PTP-CS/DA and normalized to the input of the respective sample.

Data information: Results are representative of at least two independent experiments.

substrate to the active site of the phosphatase domain, is only dependent on the Y820 residue of FGD5. We assume that residual interactions between both proteins are potentially due to additional sites on VE-PTP outside the active center of the phosphatase domain. Collectively, these results suggest that Y820 of FGD5 is a direct tyrosine substrate for VE-PTP, which is of dominant importance among the 34 tyrosine residues of this protein for its interaction with VE-PTP.

Y820 of FGD5 is necessary to counteract thrombin-induced permeability by VE-PTP inhibition

The identification of Y820 as the target tyrosine residue for VE-PTP enabled us to test whether tyrosine phosphorylation of FGD5 is relevant for the effects that VE-PTP has on junction stabilization. To clarify this, we blocked the expression of endogenous FGD5 in HUVEC by siRNA transfection, plated them on Transwell filters, and transduced them with adenoviral vectors to express either FGD5-WT-EGFP or FGD5-Y820F-EGFP. Prior to the assay, cells were pre-treated with AKB-9785 before they were challenged with thrombin and paracellular permeability was analyzed with 250 kD FITC-dextran. We found that AKB-9785 protected endothelial cells from the barrier-disruptive effect of thrombin when recombinant FGD5-WT was expressed (Fig 8A). Transduction of FGD5-Y820F, however, blocked this protective effect. The expression levels of mutant and FGD5-WT were similar (Fig 8B). Thus, Y820 of FGD5 is essential for the barrier-protective effect of VE-PTP inhibition.

Since FGD5 is considered to be a GEF for Cdc42 and Tie-2 stimulation leads to Cdc42 activation (Fig 3F), we tested whether Y820 is also needed for Cdc42 activation by FGD5 upon inhibition of VE-PTP.

Hence, we tested whether loss of endogenous FGD5 would interfere with AKB-9785-induced activation of Cdc42 and whether the result would be different if the expression of FGD5 would be rescued by transduction with FGD5-WT or FGD5-Y820F. We found that AKB-9785 enhanced Cdc42 activity in HUVEC by 66% (±27%) if cells were treated with control siRNA, whereas the increase was only 11% (±9%) if the VE-PTP inhibitor was added to cells transfected with FGD5 siRNA. Re-expression of WT-FGD5-EGFP rescued AKB-9785-induced Cdc42 activation and induced it by 70% (±18%). Strikingly, no increase in Cdc42 activity was detected upon expression of FGD5-Y820F-EGFP (Fig 8C). Expression levels of endogenous and transduced forms of FGD5 were controlled by immunoblotting (Fig 8D). We conclude that the phosphorylation of FGD5 at Y820 is required for the AKB-9785-stimulated function of FGD5 as GEF for Cdc42.

Finally, we tested whether Y820 was also needed for the effects of FGD5 on the actin cytoskeleton. HUVEC depleted for FGD5 by siRNA were transduced with either FGD5-WT-EGFP or FGD5-Y820F-EGFP and were tested for effects of thrombin and AKB-9785 on the formation of radial stress fibers or cortical actin bundles. As shown in Fig 8E, Y820 of FGD5 was needed for the induction of cortical actin bundles and the repression of radial stress fibers by AKB-9785. Since it has been reported [33] that FGD5 can bind to Radil, we tested whether FGD5 phosphorylation is needed for this interaction. Since the endogenous expression levels in endothelial cells were too weak for a successful co-precipitation, we co-expressed either FGD5-WT-EGFP or FGD5-Y820F-EGFP in HEK293 cells together with Radil-His and (for proper phosphorylation of FGD5) with Tie-2-FLAG. We found that Radil could be co-precipitated with FGD5, but this interaction was seen independent of the presence of Y820 or the phosphorylation induced by Tie-2 (Fig EV5).
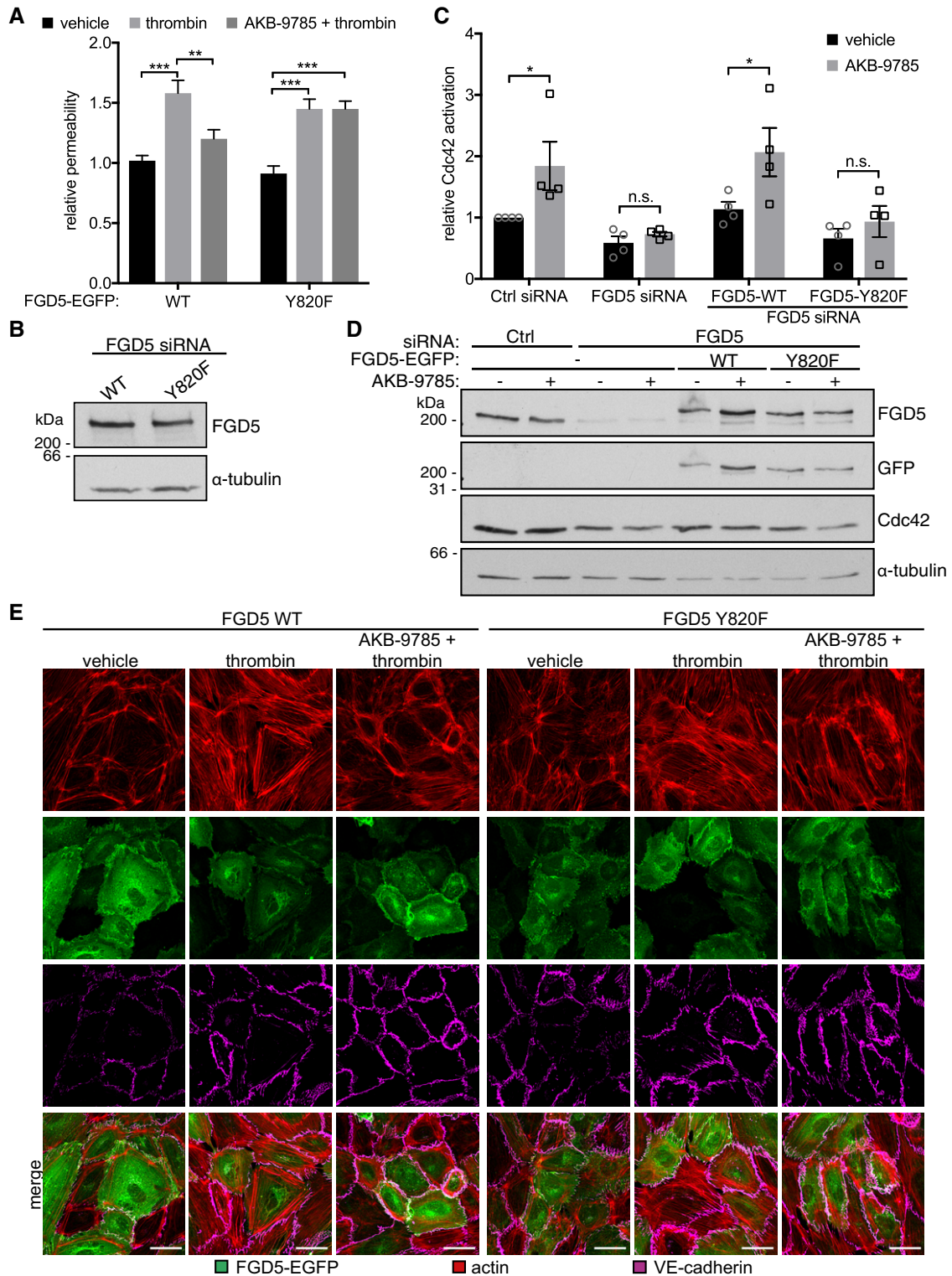
Figure 8.

Y820 is not required for the recruitment of FGD5 to endothelial junctions

We have shown above that recruitment of FGD5 to endothelial junctions is triggered by 007/Epac1-mediated activation of Rap1,

although this stimulus does not induce tyrosine phosphorylation of FGD5. This indicated that tyrosine phosphorylation of FGD5 is not needed for its junction recruitment. This would suggest that Y820 would not be needed for the AKB-9785-induced junction recruitment of FGD5. To test this, we blocked the expression of endogenous

FGD5 in HUVEC by siRNA; re-expressed either FGD5-WT-EGFP or FGD5-Y820F-EGFP with adenovirus vectors; stimulated the cells with vehicle, 007, or AKB-9785; and analyzed the cell distribution of FGD5 upon indirect immunofluorescence and confocal microscopy. As shown in Fig 9A, junction recruitment with both stimuli was detected for each of the two forms of FGD5 and for both types of stimuli. To compare the translocation efficiencies of both forms of FGD5, the signal intensities at cell contacts were quantified. Since the expression levels of adenovirus-transduced fusion proteins differed from cell to cell, fluorescence intensity detected over a length of 10 μm at cell contacts was normalized to the mean fluorescence intensity within the cytoplasm of the respective cell. Quantification revealed no significant difference between FGD5-WT and FGD5-Y820F (Fig 9B).

Discussion

Blocking the function of VE-PTP boosts the activation of Tie-2, which leads to the stabilization of the endothelial barrier function and inhibits inflammation-induced vascular leak formation. Here, we show that the GEF FGD5 is a substrate of VE-PTP, which acts downstream of VE-PTP and Tie-2. We found that FGD5 is required *in vitro* and *in vivo* in the mouse skin for the protective effect of VE-PTP inhibition on vascular barrier integrity. VE-PTP inhibition and Tie-2 activation affect FGD5 in two ways: By activating Rap1, FGD5 becomes translocated to endothelial junctions. In addition, FGD5 becomes phosphorylated at Y820, which represents a second step that is needed for full activation and the function of FGD5. Activation of FGD5 has two effects on the actomyosin system. First, it leads to activation of Cdc42 and the kinase MRCK, which promote the formation of cortical actin bundles at cell contacts and the accumulation of S19 monophosphorylated MLC at these sites. Second, radial stress fiber formation is inhibited together with the suppression of phosphorylation of MLC at T18 and S19. Thus, with FGD5 we have identified a novel signaling step downstream of VE-PTP/Tie-2, which is essential for the stabilization of endothelial junctions.
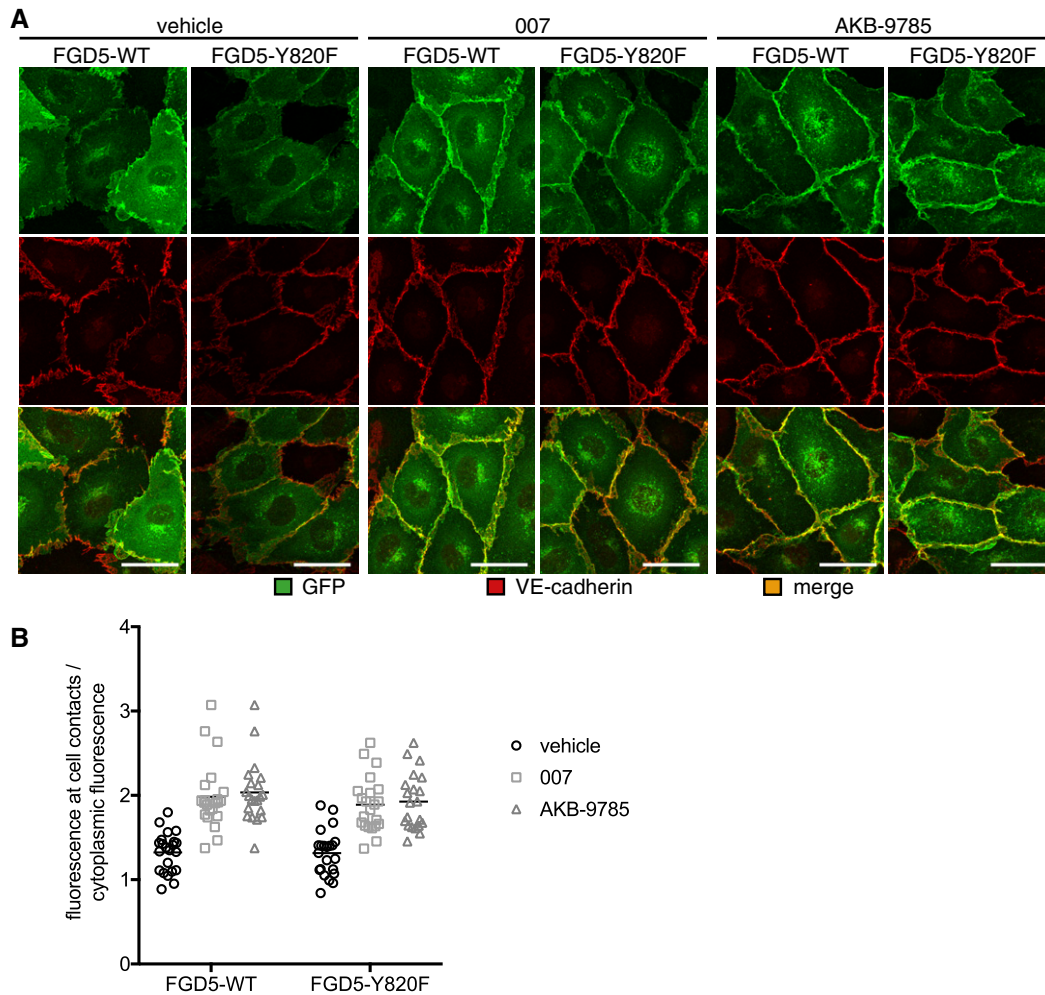
We propose that FGD5 is a direct substrate of VE-PTP since: First, a trapping mutant of the phosphatase domain of VE-PTP but not the WT form of this enzyme could affinity-isolate FGD5, demonstrating that the nature of this interaction is based on an enzyme–substrate interaction. Second, this interaction was dependent on the presence of Y820 in FGD5. The nature of FGD5 as a substrate of VE-PTP implies that inhibition of VE-PTP supports FGD5 phosphorylation by neutralizing its dephosphorylation. In addition, inhibition of VE-PTP enhances the activation of Tie-2, which in turn provides (or stimulates) the kinase activity that drives the phosphorylation of FGD5. Thus, VE-PTP inhibition supports the phosphorylation of FGD5 in two ways, by stimulating the addition and by blocking the removal of a phosphate group at Y820 of FGD5. This dual effect makes VE-PTP an attractive target for potentially existing endogenous ligands that might preserve endothelial junction stability by binding to the extracellular domain of VE-PTP and inhibiting its activity. It is still an open question whether RPTPs have ligands and up to now very few ligands for RPTPs have been identified [38,39]. It has been shown, though, that ligands for RPTPs are able to deactivate their phosphatase activity due to dimerization [40–44]. It would be interesting to find out whether such a ligand for VE-PTP exists.

Interference with the expression of Tie-2 strongly reduced the AKB-9785-induced phosphorylation of FGD5, which suggests that either Tie-2 itself or a kinase-activated downstream of Tie-2 is responsible for the phosphorylation of Y820 of FGD5. Since silencing of Tie-2 had been highly efficient, whereas the phosphorylation of FGD5 had only been inhibited by about 50%, it is possible that another kinase is also involved in the phosphorylation of FGD5. The FGD family member FRG, which is much shorter in size and varies considerably in structure, is phosphorylated by Src at yet unidentified tyrosine residues [45]. However, we did not find that inhibition of Src attenuated AKB-9785-induced FGD5 phosphorylation (Appendix Fig S1). This is consistent with the finding that Src activity was not substantially affected in endothelial cells by VE-PTP inhibition [9].

According to our results, FGD5 activation is a two-step process, which requires translocation to cell junctions and phosphorylation of Y820. Recruitment of FGD5 to junctions was triggered by the activation of Tie-2, which in turn activated Rap1. Tie-2 and Rap1 are downstream targets of VE-PTP inhibition, which are essential for junction stabilization, as we have shown previously [9]. Interestingly, silencing of Rap-1 did not affect the phosphorylation of FGD5 while it blocked junction recruitment. This suggests that junction translocation of FGD5 was not needed for its phosphorylation. In addition, the Y820F mutant of FGD5 was as efficiently translocated to junctions upon Rap1 activation as the WT form of FGD5. Thus, each activation step, junction recruitment, and tyrosine phosphorylation are mutually independent of each other.

Rap1 is a central player in signaling pathways that stabilize endothelial junctions. Several studies reported that elevation of

A

vehicle | 007 | AKB-9785

FGD5-WT | FGD5-Y820F | FGD5-WT | FGD5-Y820F | FGD5-WT | FGD5-Y820F

GFP   VE-cadherin   merge

B

Figure 9. **FGD5 translocation to cell junctions is independent of Y820.**

A   HUVEC treated with FGD5-targeting siRNA and transduced with FGD5-WT-EGFP or FGD5-Y820F-EGFP adenoviruses were treated with vehicle, 200 μM 007, or 5 μM AKB-9785, fixed, permeabilized, and stained for GFP and VE-cadherin. Scale bars 30 μm.

B   Images as shown in (A) were analyzed for GFP signal intensities determined over a length of 10 μm along junctions and normalized to the mean GFP signal intensity of the cytoplasmic area. Results are presented as individual values and mean.

Data information: Results are representative of two independent experiments (A) or pooled from two independent experiments with a total number of 20–25 cell contacts analyzed (B).

cytosolic cAMP levels stimulated linearization and stabilization of endothelial junctions by activating Epac, which in turn activated Rap1 and thereby supported the formation of cortical actin bundles [26–29]. Analyzing this in more detail, it was shown that Rap1 induces FGD5-dependent Cdc42 activation at junctions to locally activate NMII through MRCK, thereby supporting circumferential actin bundles [30,33]. In addition, Rap1 activation was found to suppress RhoA and ROCK-mediated activation of NMII at radial stress fibers [30,32,37]. In contrast to the group of Mochizuki [30], Pannekoek *et al* [33] only found a minor contribution of FGD5 to the junction stabilization effect by the cAMP analogue 007. Furthermore, FGD5 has only been described as relevant for the supportive effect of Rap1 on cortical actin bundles. Our results show that upon inhibiting VE-PTP (and activating Tie-2), FGD5 is, in addition, also needed for the inhibitory effect of Rap1 on radial stress fibers. Moreover, silencing FGD5 had a very strong inhibitory effect on junction

stabilization. We believe that we observed such a dramatic relevance of FGD5 for junction stabilization, because the full capacity of activated FGD5 as a stabilizer of endothelial junctions can only be observed if stimuli are analyzed which trigger junctional recruitment of FGD5 plus tyrosine phosphorylation of FGD5. Only both these steps fully activate FGD5. This cannot be achieved, if the cellular stimuli are limited to the use of a cAMP analogue or of reagents which simply enhance cytosolic cAMP levels.

It will be interesting to determine how FGD5 inhibits the RhoA and ROCK-mediated activation of NMII of radial stress fibers. Tie-2 was reported to inhibit radial stress fibers by activating Rac1 [22,25]. We showed previously that Tie-2 mediates these effects by activating Rap1, which then activates Rac1 [9]. FGD5 was described as a GEF for Cdc42. Here, we have shown that FGD5 is also needed for AKB-9785-induced activation of Rac1, and this activity of FGD5 did not require the expression of Cdc42. This may suggest that

FGD5 could even act as GEF for Rac1, although, to formally demonstrate this, enzyme assays with the purified proteins would need to be performed. Even if FGD5 is not directly acting as a GEF for Rac1, it is obviously needed for Tie-2-stimulated Rac1 activation which could explain how FGD5 counteracts RhoA and ROCK-mediated activation of NMII of radial stress fibers.

FGD5 has been described as specifically expressed in endothelial cells [35,36] and hematopoietic stem cells, while being absent in leukocytes of the periphery [34]. In the developing zebrafish and mouse embryos, FGD5 transcripts were specifically detected by *in situ* hybridization in Flk1-positive cell populations along the vascular tree similar to endothelial markers such as PECAM-1 [35,36]. Given that FGD5 is specifically expressed in endothelial cells, our *in vivo* siRNA experiments clearly indicate that *in vivo*, FGD5 is required in endothelial cells for the protective role of Tie-2 against inflammation-induced vascular leakage. It is remarkable that three key players of this signaling pathway, VE-PTP, Tie-2, and FGD5, are highly selective for endothelium. This highlights the importance of this pathway for the plasticity and flexibility of endothelial junction integrity, which is a hallmark for the highly dynamic regulation of the barrier function of the blood vessel wall.

The importance of VE-PTP for the regulation of endothelial junctions is further highlighted by the fact that from the 47 proteins we detected to harbor 56 tyrosine phosphosites stimulated by the VE-PTP inhibitor, 13 were proteins, which have been implicated in the regulation of junctions. It will be interesting to investigate in the future whether these proteins are indeed involved in mechanisms whereby VE-PTP influences endothelial junction stability.

In conclusion, our results establish FGD5 as an essential signaling target of VE-PTP, which is *in vitro* and *in vivo* required for the stabilization of endothelial junctions by VE-PTP inhibition and Tie-2 activation. We found that FGD5 is a direct substrate of VE-PTP and at the same time a target for Tie-2-stimulated (direct or indirect) phosphorylation. The identification of Y820 as the single substrate tyrosine of human FGD5 activation established this modification as an essential aspect of full activation of FGD5. This enabled us to show that fully activated FGD5 is required to support tension of circumferential actin bundles as well as to relieve tension of radial stress fibers. Collectively, these results establish FGD5 as a new component of the signaling mechanism whereby VE-PTP/Tie-2 protect the vasculature against plasma leakage.

Materials and Methods

Antibodies and reagents

Rabbit polyclonal antibody VD68/FGD5 N-term was raised against and affinity-purified on a bacterial fusion protein containing glutathione S-transferase (GST) fused to amino acids 1–248 of murine FGD5. Specific antibodies were depleted for anti-GST antibodies prior to use. The polyclonal VE-PTP-C antibody against VE-PTP [10] and 3G1 against Tie-2 [46] have been described previously. The following antibodies were commercially obtained: monoclonal antibodies against phospho-tyrosine (4G10) and human Tie-2 (Tek33.3; both Merck Millipore), human Cdc42 (44/CDC42; BD Bioscience), α-tubulin (B-5-1-2; Sigma-Aldrich), human VE-cadherin (F-8; Santa Cruz Biotechnology, Inc.), Rac1 (Cytoskeleton), and 6x-His-Tag (His.H8;

Thermo Scientific), as well as polyclonal antibodies against human FGD5 (B01P from Abnova or from Proteintech); GST (Z-5), human VE-cadherin (C-19), and human PECAM-1 (M-20; Santa Cruz Biotechnology, Inc.); Rap1 (Merck Millipore); pMLC-2 S19 and pMLC-2 T18/S19 (Cell Signaling Technology); GFP (Abcam); and FLAG-tag (Sigma-Aldrich). HRPO-coupled secondary antibodies were purchased from Dianova. Alexa Fluor 488-, Alexa Fluor 568-, and Alexa Fluor 647-coupled antibodies, as well as phalloidin-Alexa Fluor 568 or phalloidin-Alexa Fluor 647, were purchased from Invitrogen.

The VE-PTP inhibitors AKB-9785 and AKB-9778 are equivalent in specificity and inhibitory activity (Aerpio Pharmaceuticals) and were used as 10 mM (6.07 mg/ml) stock solutions in 5% glucose. The following additional reagents were used: human thrombin (EMD Millipore), histamine (Sigma-Aldrich), COMP-Ang1 (G.Y. Koh), human Ang1 (R&D Systems), 8-pCPT-2′-O-Me-cAMP (007; Tocris Bioscience), fluorescent mounting medium (Dako), and 250 kD FITC-dextran (Sigma-Aldrich).

Phospho-peptide enrichment

Changes of protein phosphorylation upon phosphatase inhibition on a global level were performed with confluent bEnd.5 cells (5 × 15 cm dishes), which were treated with AKB-9778 (50 μM, 30 min), lysed in RIPA buffer supplemented with protease (Complete, Roche) and phosphatase inhibitors (PhosSTOP, Roche), and then subjected to the filter-aided sample preparation procedure (FASP) as described [47] using Amicon Ultra-15 ultrafiltration units (nominal molecular weight cutoff 30 kDa). Briefly, following reduction of disulfide bridges by the addition of 0.1 M DTT (45 min at 56°C) and alkylation by iodoacetamide (55 mM, 20 min at RT in the dark), the sample was first digested with trypsin (100 μg/10 mg protein) for 3 h at 37°C, after which additional trypsin was added (100 μg/10 mg protein) and the incubation continued overnight. Peptides were harvested by centrifugation. Following adjustment of the pH value of the filtrate to pH 2.5 by the addition of TFA, acetonitrile (ACN) was added to a final concentration of 30%. Acidified peptides were subjected to strong anion exchange chromatography on a Resource S column (GE Healthcare) using sample loading via a superloop and an Äkta Explorer Chromatography System (Buffer A: 7 mM KH_2PO_4, 30% ACN; Buffer B: 7 mM KH_2PO_4, 30% ACN, 350 mM KCl; gradient from 0 to 30% B in 30 min, 100% B for 10 min, flow rate 2 ml/min). Fractions were pooled according to the elution profile (flow-through fraction + 9 pools). Phospho-peptides from each pool were enriched using TiO_2 microspheres (GL Sciences) in the presence of DHB. Each pool was extracted twice by the addition of TiO_2 beads (3 mg/pool) that had been pre-equilibrated in loading buffer (6× stock: 30 mg/ml DHB, 80% ACN) for 20 min at RT on a rotary shaker. TiO_2 suspensions were then transferred to double-layer C8 Stage-Tips, which were washed with 30% ACN, 3% TFA and 80% ACN, 0.3% TFA. Phospho-peptides were finally eluted with 40% ACN, 60% NH_4OH, concentrated to a volume of ~3 μl in a vacuum concentrator, and acidified by the addition of 0.5% acetic acid prior to injection into the mass spectrometer.

Nano-LC-MS/MS analysis

Each phospho-peptide pool was fractionated on in-house packed fused silica capillary columns (length 15 cm; ID 75 μm; resin

ReproSil-Pur C18-AQ, 3 μm) using a Proxeon EASY-nLC high-pressure liquid nanoflow chromatography system that was coupled via a Proxeon electrospray ion source to an LTQ-Orbitrap Velos Mass Spectrometer. Bound peptides were eluted using a linear 120 min gradient from 5 to 35% B (80% ACN, 0.5% acetic acid) followed by a gradient from 35 to 98% B in 15 min. All phospho-peptide-containing fractions were measured with the mass spectrometer operated in positive mode and (i) with multistage activation (pseudo MS3) enabled, triggering activation of the neutral loss species at 97.97, 48.99, or 32.66 m/z below the precursor ion of the 15 most intense ions for 10 ms (survey scans from m/z 300 to 1,800 at $R = 30,000$), and (ii) in HCD mode (higher-energy collisional dissociation; survey scans from m/z 300 to 1,600 at $R = 30,000$, fragmentation of 10 most intense peptide ions at a normalized collision energy of 40% and detection in the Orbitrap cell at $R = 7,500$). Raw MS data were processed using MaxQuant (v. 1.5.3.8) with the built-in Andromeda search engine. Tandem mass spectra were searched against the mouse UniProtKB database (UP000000589_10090_mm.fasta; version from 12/2015) concatenated with reversed sequence versions of all entries and also containing common contaminants. Carbamidomethylation was set as fixed modification for the search in the database, while oxidation at methionine, acetylation of the protein N-termini, and phosphorylation at Ser, Thr, and Tyr were allowed as variable modifications. Trypsin was defined as the digesting enzyme, allowing a maximum of two missed cleavages and requiring a minimum length of 7 amino acids. The maximum allowed mass deviation was 20 ppm for MS and 0.5 Da for MS/MS scans. Protein groups were regarded as being unequivocally identified with a false discovery rate (FDR) of 1% for both the peptide and protein identifications. Phosphosites were accepted when they were identified with a localization probability of > 0.75 and a score difference > 5 (class I phosphosites). Tables containing all identified proteins with accession numbers, gene names, and corresponding quantitative values are available as Dataset EV1.

DNA constructs

The pEGFP-C1-FGD5 plasmid was provided by Naoki Mochizuki via Addgene. The Y820F mutation as well as three silent mutations in the siRNA-binding sequence (changing 5′-TGACATGGAC-3′ to 5′-CGATATGGAT-3′) was introduced using the QuikChange Lightning Site-directed Mutagenesis Kit (Agilent Technologies). Adenoviruses containing siRNA-insensitive FGD5-WT-EGFP or FGD5-Y820F-EGFP were generated using the ViraPower Expression System (Invitrogen) by subcloning of sequences into the gateway vector pENTR2B (Invitrogen) and site-specific recombination into the pAd/CMV-DEST destination vector (Invitrogen). pCMV6-Tie2-Myc-DDK and pCMV6-Radil-Myc-DDK were purchased via OriGene, and the pCDNA3.1/myc-His(-)A-Radil plasmid was obtained by subcloning of the Radil sequence into the pcDNA3.1/myc-His(-)A vector (Invitrogen).

Cell culture and transient transfection

HUVEC were cultured in EBM-2 medium supplemented with SingleQuots (Lonza) or in ECGM-2 medium supplemented with SupplementPack (PromoCell). bEnd.5 endothelioma cells were grown in Dulbecco's modified Eagle's medium supplemented with 10% FCS, 2 mM L-glutamine, 1 mM sodium pyruvate, 1% non-essential amino acids, and 1% penicillin/streptomycin. HEK293A cells were cultured in Dulbecco's modified Eagle's medium supplemented with 10% FCS, 2 mM L-glutamine, 1% non-essential amino acids, and 1% penicillin/streptomycin. Transient transfections were performed using the GeneJammer Transfection Reagent (Agilent) according to the manufacturer's instructions. Cells were subjected to experiments 48 h after transfection.

RNA interference and adenoviral re-expression

For in vitro RNA interference with expression of FGD5, Tie-2, Rap1, or VE-PTP, the following siRNAs were used: Hs_FGD5_6, 5′-GCGC UGACACUUCAGACUA-3′ or Hs_FGD5_2, 5′-GGAUGACAUGGACCAU GAA-3′ (targeting human FGD5, QIAGEN); Hs_Tek_6, 5′-GGUGCUAC UUAACAACUUA-3′ (targeting human Tie-2, QIAGEN); ON-TARGETplus Rap1A (5906), 5′-GCAAGACAGUGGUGUAACU-3′ (human Rap1A) and Rap1B (5908), 5′-GGACAAGGAUUUGCAUUAG-3′ (human Rap1B, both Dharmacon, GE Healthcare; and a combination of Hs_PTPRB_5, 5′-UAACUUGAUAAAGUCGACCGG-3′ and Hs_PTPRB_10, 5′-UAUCGU UCCACAUUCCCAGAA-3′ (both targeting human VE-PTP, QIAGEN). As a negative control, siRNA that does not target any known mammalian gene was used (5′-UUCUCCGAACGUGUCACGU-3′, QIAGEN). Routinely, 10^6 HUVEC were transfected with 30–50 nm siRNA using INTERFERin (Polyplus Transfection) according to the manufacturer's instructions. Cells were analyzed 24 h (VE-PTP), 48 h (Tie-2), or 72 h (FGD5, Rap1A/B) after transfection.

Adenoviral transduction was used to re-introduce FGD5 after siRNA-mediated knockdown. HUVEC were infected with adenovirus encoding FGD5-WT-EGFP and FGD5-Y820F-EGFP, respectively, once 40 h and a second time 16 h prior to the experiment.

For RNA interference with FGD5 expression in vivo, the siRNA 5′-CAGUCGGUGUAUAGUUAGUAA-3′ was used. The sequence was provided by QIAGEN (Mm_FGD5_4), tested in vitro, and modified for higher stability for in vivo applications by Dharmacon (siSTABLE, GE Healthcare). As a negative control, siRNA that does not target any known mammalian gene was modified identically (5′-TAGCGACTAAACACATCAA-3′; siSTABLE; GE Healthcare). Mice were injected i.v. with 60 μg siRNA using in vivo jetPEI as transfer reagent (Polyplus Transfection) according to the manufacturer's instructions and analyzed 48 h later.

Immunoprecipitation and immunoblotting

For detection of phospho-tyrosine after immunoprecipitation, cells were lysed in lysis buffer containing 20 mM Tris–HCl, pH 7.4, 150 mM NaCl, 2 mM $CaCl_2$, 1.5 mM $MgCl_2$, 1 mM Na_3VO_4, 1% Triton-X-100, 0.04% NaN_3, and 1× Complete EDTA-free proteinase inhibitors (Roche). Lysates were centrifuged at 20,000 g and 4°C for 1 h before aliquots for direct blot analysis were set aside and aliquots for immunoprecipitation were incubated for 2 h at 4°C with protein-A/G-Sepharose loaded with the respective antibodies. Immunocomplexes were washed five times with lysis buffer. Murine lungs were homogenized using Ultra-Turrax (IKA-Werke) or Precellys Evolution (Bertin Instruments) in RIPA buffer containing 1% NP-40, 1% sodium deoxycholate, 0.01 M NaPi, 150 mM NaCl, 2 mM EDTA, 1 mM Na_3VO_4, and 2× Complete EDTA-free protease inhibitors. Immunocomplexes and lysates were analyzed by SDS–PAGE. Total cell or organ lysates or immunoprecipitated material

was subjected to SDS–PAGE and transferred to nitrocellulose (Schleicher & Schuell) by wet blotting. Blots were analyzed as described previously [48]. For detection of phosphorylated tyrosine, milk powder in the blocking buffer was replaced by 2% BSA and 200 μM Na_3VO_4 was added.

Immunofluorescence staining

HUVEC were seeded on fibronectin-coated chamber slides (LabTek, 8-well, glass) and grown to confluence. They were stimulated with AKB-9785 for 20–30 min, 007 for 20 min, thrombin for 2, 15 or 30 min, and Ang1 for 20 min. Cells were washed with PBS, fixed with 4% PFA/PBS for 7 min at room temperature, permeabilized using 0.5% Triton X-100/PBS for 5 min at room temperature, and blocked with 3% BSA for 1 h, followed by incubation with primary antibodies. Primary antibodies were detected with Alexa Fluor 488-, Alexa Fluor 568-, or Alexa Fluor 647-coupled secondary antibodies. Phalloidin-Alexa Fluor 568 or phalloidin-Alexa Fluor 647 was added to detect filamentous actin during incubation with secondary antibodies. Z-stack projections were acquired using a Zeiss LSM 780 confocal microscope and analyzed with ImageJ and ZEN software (Zeiss). To quantify FGD5 cell-contact recruitment or VE-cadherin intensity at cell–cell junctions, fluorescence intensity was measured over a length of 10 μm along junctions and normalized to the mean fluorescence intensity of the cytoplasmic area. In cells re-transfected to overexpress FGD5, only cell contacts formed by two cells with similar FGD5 expression levels were quantified. When brightness and contrast were adjusted, same processing was applied to images of all conditions.

VE-PTP substrate trapping

For substrate-trapping pull-down experiments, bEnd.5 cells or HUVEC were treated with 100 μM peroxyvanadate for 7 min and lysed in 20 mM Tris–HCl, pH 7.5, 100 mM NaCl, 1 mM EDTA, 1% Triton X-100, 10% glycerin, 5 mM iodoacetic acid (IAA), and 1× Complete EDTA-free protease inhibitor cocktail (Roche) for 30 min at 4°C. Subsequently, 10 mM DTT was added to inactivate IAA. After centrifugation at 20,000 g for 30 min at 4°C, lysates were pre-cleared by incubation with 5 μg GST bound to glutathione Sepharose for 1–3 h at 4°C and subsequently incubated with 10 μg GST, GST-VE-PTP, or GST-VE-PTP-CS/DA bound to glutathione Sepharose, as previously described [49]. Beads were washed five times in 1 ml of lysis buffer and were analyzed by SDS–PAGE and immunoblotting.

GTPase activation assays for Cdc42 and Rac1

HUVEC were serum-starved overnight in the presence of 1% BSA followed by starvation for 3 h without BSA. Cells were stimulated with 5 μM AKB-9785, 200 μM 007, or 600 ng/ml Ang1 for 20 min before they were lysed and used to perform a G-LISA Cdc42 or Rac1 activation assays (colorimetric format, Cytoskeleton, Inc.) according to the manufacturer's instructions. In brief, lysates were cleared by centrifugation at 20,000 g and 4°C for 1 min, protein concentrations were equalized to a total protein concentration of 0.25 mg/ml, and lysates were incubated with the respective GTPase-GTP affinity plate for 15 min. After labeling with Cdc42 or Rac1 antibodies and

HRP-coupled secondary antibodies, levels of GTP-loaded Cdc42 or Rac1 were determined by reading OD490 nm in a 96-well plate reader (Synergy 2, BioTek).

In vitro permeability assay

To determine paracellular permeability, HUVEC were transfected with siRNA, and 1 day later, 2×10^4 cells were seeded on 100 μg/ml fibronectin-coated Transwell filters (6.5 mm, 0.4 μm pore size, Corning) and grown to confluence. For stimulation, HUVEC were serum-starved for 2–3 h and pre-incubated with 5 μM AKB-9785 or vehicle for 30 min, followed by stimulation with 1–2 U/ml thrombin for 45 min parallel to the diffusion of 0.25 mg/ml FITC-dextran (250 kD Sigma-Aldrich) at 37°C and 5% CO_2. Basal monolayer permeability for 250 kD FITC-dextran was determined without any stimulation for 45 min at 37°C and 5% CO_2. Fluorescence in the lower chamber was measured in a plate reader (Synergy 2, LabTek), and monolayer integrity was confirmed by immunostaining for VE-cadherin after each assay.

Electric cell–substrate impedance sensing

1×10^5 HUVEC were seeded onto L-cysteine-reduced, fibronectin-coated 8W10E electrodes (Applied Biophysics). Twenty-four hours after siRNA transfection, electrical impedance was measured in real time at 37°C and 5% CO_2 using the ECIS ZΘ system (Applied Biophysics) at 4,000 Hz. Forty-eight hours after seeding, cells were serum-starved for 3 h, pre-incubated with 5 μM AKB-9785 or 1 μg/ml COMP-Ang1 for 30 min, and stimulated with 1–2 U/ml thrombin.

In vivo permeability assay in the skin

One hour before the assay, 8–12-week-old female mice were injected subcutaneously with vehicle or AKB-9785 (0.6 mg per injection). Then, a modified Miles assay for the induction of vascular permeability in the skin was performed as described previously [50]. Evans blue dye (Sigma-Aldrich) was injected into the tail vein (100 μl of a 1% solution in PBS), and after 15 min, 50 μl PBS or 225 ng histamine in 50 μl PBS was injected intradermally into the shaved back skin. Then, 30 min later, skin areas were excised and extracted with formamide for 5 days, and the concentration of the dye was measured at 620 nm with a spectrophotometer (Shimadzu). All animal experiments were approved by the Landesamt für Natur, Umwelt und Verbraucherschutz Nordrhein-Westfalen. Animals were kept in a barrier facility under special pathogen-free conditions.

RNA isolation and quantitative real-time PCR

Total RNA was isolated from HUVEC transfected with FGD5 or control siRNA using the RNeasy Mini Kit (QIAGEN) and reverse-transcribed to cDNA using SuperScript II Reverse Transcriptase (Invitrogen). Obtained cDNA samples were subjected to quantitative real-time PCR using iTaq Universal SYBR Green Supermix (Bio-Rad), and cDNA levels were measured on a 7300 Real Time PCR System (Applied Biosystems) using pre-designed KiCqStart SYBR Green Primers (Sigma-Aldrich): CAAACAGGGAAGATGAAGAC and GTGATAGAATTGAAGGGCTC (human FGD1), CAGAAGATACCA ATTCAGCTC and AAGTCCACATGCTTGATAAC (human FGD5), GA

AGTATCAGCAAACACAGAG and GACAAACCAAAAGTGTTTCC (human FGD6), and ACAGTTGCCATGTAGACC and TTGAGCACA GGGTACTTTA (human GAPDH). Gene expression of FGD proteins was normalized to GAPDH levels and displayed relative to expression levels in control siRNA-treated cells.

Statistical analysis

Datasets were tested for normality (Shapiro–Wilk) and equal variance. Statistical significance was analyzed using two-tailed Student's *t*-test, one-way ANOVA, or two-way ANOVA for independent samples. Turkey's multiple comparison test was applied to correct for multiple comparisons. GraphPad Prism7 software was used for this analysis. *P*-values are indicated by asterisks: *$P < 0.05$; **$P < 0.01$; and ***$P < 0.001$. Results are shown as means $\pm$ SEM. Immunoblot signals were quantified using the software Multi-Gauge V3.2 (Fuji) or ImageJ.

Data availability

All mass spectrometric data have been deposited to the ProteomeXchange Consortium (http://proteomecentral.proteomexchange.org) via the PRIDE [51] partner repository with the dataset identifier PXD010959.

Expanded View for this article is available online.

Author contributions

LJB, MZ, MV, and HCD performed, analyzed, and designed the experiments; KP provided essential reagents; and DV initiated the study, designed the experiments, and wrote the manuscript.

Conflict of interest

D. Vestweber serves on the Scientific Advisory Board for Aerpio Therapeutics. K. Peters is an employee of Aerpio Therapeutics. The authors declare that they have no conflict of interest.

References

1. Dejana E (2004) Endothelial cell-cell junctions: happy together. *Nat Rev Mol Cell Biol* 5: 261–270
2. Vestweber D (2008) VE-cadherin: the major endothelial adhesion molecule controlling cellular junctions and blood vessel formation. *Arterioscler Thromb Vasc Biol* 28: 223–232
3. Dejana E, Vestweber D (2013) The role of VE-cadherin in vascular morphogenesis and permeability control. In *The molecular biology of cadherins*, van Roy F (ed.), pp 119–144. Amsterdam: Elsevier
4. Carmeliet P, Lampugnani M-G, Moons L, Breviario F, Compernolle V, Bono F, Balconi G, Spagnuolo R, Oosthuyse B, Dewerchin M *et al* (1999) Targeted deficiency or cytosolic truncation of the VE-cadherin gene in mice impairs VEGF-mediated endothelial survival and angiogenesis. *Cell* 98: 147–157
5. Gory-Faure S, Prandini MH, Pointu H, Roullot V, Pignot-Paintrand I, Vernet M, Huber P (1999) Role of vascular endothelial-cadherin in vascular morphogenesis. *Development* 126: 2093–2102
6. Gotsch U, Borges E, Bosse R, Böggemeyer E, Simon M, Mossmann H, Vestweber D (1997) VE-cadherin antibody accelerates neutrophil recruitment *in vivo*. *J Cell Sci* 110: 583–588
7. Corada M, Mariotti M, Thurston G, Smith K, Kunkel R, Brockhaus M, Lampugnani MG, Martin-Padura I, Stoppacciaro A, Ruco L *et al* (1999) Vascular endothelial-cadherin is an important determinant of microvascular integrity *in vivo*. *Proc Natl Acad Sci USA* 96: 9815–9820
8. Schulte D, Küppers V, Dartsch N, Broermann A, Li H, Zarbock A, Kamenyeva O, Kiefer F, Khandoga A, Massberg S *et al* (2011) Stabilizing the VE-cadherin-catenin complex blocks leukocyte extravasation and vascular permeability. *EMBO J* 30: 4157–4170
9. Frye M, Dierkes M, Küppers V, Vockel M, Tomm J, Zeuschner D, Rossaint J, Zarbock A, Koh GY, Peters K *et al* (2015) Interfering with VE-PTP stabilizes endothelial junctions *in vivo* via Tie-2 in the absence of VE-cadherin. *J Exp Med* 212: 2267–2287
10. Nawroth R, Poell G, Ranft A, Samulowitz U, Fachinger G, Golding M, Shima DT, Deutsch U, Vestweber D (2002) VE-PTP and VE-cadherin ectodomains interact to facilitate regulation of phosphorylation and cell contacts. *EMBO J* 21: 4885–4895
11. Nottebaum AF, Cagna G, Winderlich M, Gamp AC, Linnepe R, Polaschegg C, Filippova K, Lyck R, Engelhardt B, Kamenyeva O *et al* (2008) VE-PTP maintains the endothelial barrier via plakoglobin and becomes dissociated from VE-cadherin by leukocytes and by VEGF. *J Exp Med* 205: 2929–2945
12. Vockel M, Vestweber D (2013) How T cells trigger the dissociation of the endothelial receptor phosphatase VE-PTP from VE-cadherin. *Blood* 122: 2512–2522
13. Broermann A, Winderlich M, Block H, Frye M, Rossaint J, Zarbock A, Cagna G, Linnepe R, Schulte D, Nottebaum AF *et al* (2011) Dissociation of VE-PTP from VE-cadherin is required for leukocyte extravasation and for VEGF-induced vascular permeability *in vivo*. *J Exp Med* 208: 2393–2401
14. Mellberg S, Dimberg A, Bahram F, Hayashi M, Rennel E, Ameur A, Westholm JO, Larsson E, Lindahl P, Cross MJ *et al* (2009) Transcriptional profiling reveals a critical role for tyrosine phosphatase VE-PTP in regulation of VEGFR2 activity and endothelial cell morphogenesis. *FASEB J* 23: 1490–1502
15. Hayashi M, Majumdar A, Li X, Adler J, Sun Z, Vertuani S, Hellberg C, Mellberg S, Koch S, Dimberg A *et al* (2013) VE-PTP regulates VEGFR2 activity in stalk cells to establish endothelial cell polarity and lumen formation. *Nat Commun* 4: 1672
16. Fachinger G, Deutsch U, Risau W (1999) Functional interaction of vascular endothelial-protein-tyrosine phosphatase with the angiopoietin receptor Tie-2. *Oncogene* 18: 5948–5953
17. Winderlich M, Keller L, Cagna G, Broermann A, Kamenyeva O, Kiefer F, Deutsch U, Nottebaum AF, Vestweber D (2009) VE-PTP controls blood vessel development by balancing Tie-2 activity. *J Cell Biol* 185: 657–671
18. Baumer S, Keller L, Holtmann A, Funke R, August B, Gamp A, Wolburg H, Wolburg-Buchholz K, Deutsch U, Vestweber D (2006) Vascular endothelial cell specific phospho-tyrosine phosphatase (VE-PTP) activity is required for blood vessel development. *Blood* 107: 4754–4762

19. Dominguez MG, Hughes VC, Pan L, Simmons M, Daly C, Anderson K, Noguera-Troise I, Murphy AJ, Valenzuela DM, Davis S *et al* (2007) Vascular endothelial tyrosine phosphatase (VE-PTP)-null mice undergo vasculogenesis but die embryonically because of defects in angiogenesis. *Proc Natl Acad Sci USA* 104: 3243−3248

20. Thurston G, Rudge JS, Ioffe E, Zhou H, Ross L, Croll SD, Glazer N, Holash J, McDonald DM, Yancopoulos GD (2000) Angiopoietin-1 protects the adult vasculature against plasma leakage. *Nat Med* 6: 460−463

21. Gamble JR, Drew J, Trezise L, Underwood A, Parsons M, Kasminkas L, Rudge J, Yancopoulos G, Vadas MA (2000) Angiopoietin-1 is an antipermeability and anti-inflammatory agent *in vitro* and targets cell junctions. *Circ Res* 87: 603−607

22. Mammoto T, Parikh SM, Mammoto A, Gallagher D, Chan B, Mostoslavsky G, Ingber DE, Sukhatme VP (2007) Angiopoietin-1 requires p190 RhoGAP to protect against vascular leakage *in vivo*. *J Biol Chem* 282: 23910−23918

23. Shen J, Frye M, Lee BL, Reinardy JL, McClung JM, Ding K, Kojima M, Xia H, Seidel C, Lima e Silva R *et al* (2014) Targeting VE-PTP activates TIE2 and stabilizes the ocular vasculature. *J Clin Invest* 124: 4564−4576

24. Gavard J, Patel V, Gutkind JS (2008) Angiopoietin-1 prevents VEGF-induced endothelial permeability by sequestering Src through mDia. *Dev Cell* 14: 25−36

25. David S, Ghosh CC, Mukherjee A, Parikh SM (2011) Angiopoietin-1 requires IQ domain GTPase-activating protein 1 to activate Rac1 and promote endothelial barrier defense. *Arterioscler Thromb Vasc Biol* 31: 2643−2652

26. Kooistra MR, Corada M, Dejana E, Bos JL (2005) Epac1 regulates integrity of endothelial cell junctions through VE-cadherin. *FEBS Lett* 579: 4966−4972

27. Wittchen ES, Worthylake RA, Kelly P, Casey PJ, Quilliam LA, Burridge K (2005) Rap1 GTPase inhibits leukocyte transmigration by promoting endothelial barrier function. *J Biol Chem* 280: 11675−11682

28. Cullere X, Shaw SK, Andersson L, Hirashi J, Luscinskas FW, Mayadas TN (2005) Regulation of vascular endothelial barrier function by Epac, a cAMP-activated exchange factor for Rap GTPase. *Blood* 105: 1950−1955

29. Noda K, Zhang J, Fukuhara S, Kunimoto S, Yoshimura M, Mochizuki N (2010) Vascular endothelial-cadherin stabilizes at cell-cell junctions by anchoring to circumferential actin bundles through alpha- and beta-catenins in cyclic AMP-Epac-Rap1 signal-activated endothelial cells. *Mol Biol Cell* 21: 584−596

30. Ando K, Fukuhara S, Moriya T, Obara Y, Nakahata N, Mochizuki N (2013) Rap1 potentiates endothelial cell junctions by spatially controlling myosin II activity and actin organization. *J Cell Biol* 202: 901−916

31. Pannekoek WJ, van Dijk JJ, Chan OY, Huveneers S, Linnemann JR, Spanjaard E, Brouwer PM, van der Meer AJ, Zwartkruis FJ, Rehmann H *et al* (2011) Epac1 and PDZ-GEF cooperate in Rap1 mediated endothelial junction control. *Cell Signal* 23: 2056−2064

32. Pannekoek WJ, Post A, Bos JL (2014) Rap1 signaling in endothelial barrier control. *Cell Adh Migr* 8: 100−107

33. Pannekoek WJ, Vliem MJ, Bos JL (2018) Multiple Rap1 effectors control Epac1-mediated tightening of endothelial junctions. *Small GTPases* 17: 1−8

34. Gazit R, Mandal PK, Ebina W, Ben-Zvi A, Nombela-Arrieta C, Silberstein LE, Rossi DJ (2014) Fgd5 identifies hematopoietic stem cells in the murine bone marrow. *J Exp Med* 211: 1315−1331

35. Kurogane Y, Miyata M, Kubo Y, Nagamatsu Y, Kundu RK, Uemura A, Ishida T, Quertermous T, Hirata K, Rikitake Y (2012) FGD5 mediates

proangiogenic action of vascular endothelial growth factor in human vascular endothelial cells. *Arterioscler Thromb Vasc Biol* 32: 988−996

36. Cheng C, Haasdijk R, Tempel D, van de Kamp EH, Herpers R, Bos F, Den Dekker WK, Blonden LA, de Jong R, Bürgisser PE *et al* (2012) Endothelial cell-specific FGD5 involvement in vascular pruning defines neovessel fate in mice. *Circulation* 125: 3142−3158

37. Post A, Pannekoek WJ, Ross SH, Verlaan I, Brouwer PM, Bos JL (2013) Rasip1 mediates Rap1 regulation of Rho in endothelial barrier function through ArhGAP29. *Proc Natl Acad Sci USA* 110: 11427−11432

38. Meng K, Rodriguez-Pena A, Dimitrov T, Chen W, Yamin M, Noda M, Deuel TF (2000) Pleiotrophin signals increased tyrosine phosphorylation of beta - catenin through inactivation of the intrinsic catalytic activity of the receptor-type protein tyrosine phosphatase beta/zeta. *Proc Natl Acad Sci USA* 97: 2603−2608

39. Peles E, Nativ M, Campbell PL, Sakurai T, Martinez R, Lev S, Clary DO, Schilling J, Barnea G, Plowman GD *et al* (1995) The carbonic anhydrase domain of receptor tyrosine phosphatase beta is a functional ligand for the axonal cell recognition molecule contactin. *Cell* 82: 251−260

40. Desai DM, Sap J, Schlessinger J, Weiss A (1993) Ligand-mediated negative regulation of a chimeric transmembrane receptor tyrosine phosphatase. *Cell* 73: 541−554

41. Majeti R, Bilwes AM, Noel JP, Hunter T, Weiss A (1998) Dimerization-induced inhibition of receptor protein tyrosine phosphatase function through an inhibitory wedge. *Science* 279: 88−91

42. Bilwes AM, den Hertog J, Hunter T, Noel JP (1996) Structural basis for inhibition of receptor protein-tyrosine phosphatase-a by dimerization. *Nature* 382: 555−559

43. Jiang G, den Hertog J, Su J, Noel JP, Sap J, Hunter T (1999) Dimerization inhibits the activity of receptor-like protein tyrosine phosphatase-a. *Nature* 401: 606−610

44. Fukada M, Fujikawa A, Chow JP, Ikematsu S, Sakuma S, Noda M (2006) Protein tyrosine phosphatase receptor type Z is inactivated by ligand-induced oligomerization. *FEBS Lett* 580: 4051−4056

45. Miyamoto Y, Yamauchi J, Itoh H (2003) Src kinase regulates the activation of a novel FGD-1-related Cdc42 guanine nucleotide exchange factor in the signaling pathway from the endothelin A receptor to JNK. *J Biol Chem* 278: 29890−29900

46. Koblizek TI, Runting AS, Stacker SA, Wilks AF, Risau W, Deutsch U (1997) Tie2 receptor expression and phosphorylation in cultured cells and mouse tissues. *Eur J Biochem* 244: 774−779

47. Wiśniewski JR, Zougman A, Nagaraj N, Mann M (2009) Universal sample preparation method for proteome analysis. *Nat Methods* 6: 359−362

48. Ebnet K, Schulz CU, Meyer-zu-Brickwedde M-K, Pendl GG, Vestweber D (2000) Junctional Adhesion Molecule (JAM) interacts with the PDZ domain containing proteins AF-6 and ZO-1. *J Biol Chem* 275: 27979−27988

49. Blanchetot C, Chagnon M, Dubé N, Hallé M, Tremblay ML (2005) Substrate-trapping techniques in the identification of cellular PTP targets. *Methods* 35: 44−53

50. Mamluk R, Klagsbrun M, Detmar M, Bielenberg DR (2005) Soluble neuropilin targeted to the skin inhibits vascular permeability. *Angiogenesis* 8: 217−227

51. Vizcaíno JA, Deutsch EW, Wang R, Csordas A, Reisinger F, Ríos D, Dianes JA, Sun Z, Farrah T, Bandeira N *et al* (2014) ProteomeXchange provides globally coordinated proteomics data submission and dissemination. *Nat Biotechnol* 32: 223−226